Article

Cell Metabolism

Distinct Circadian Signatures in Liver and Gut Clocks Revealed by Ketogenic Diet

Graphical Abstract

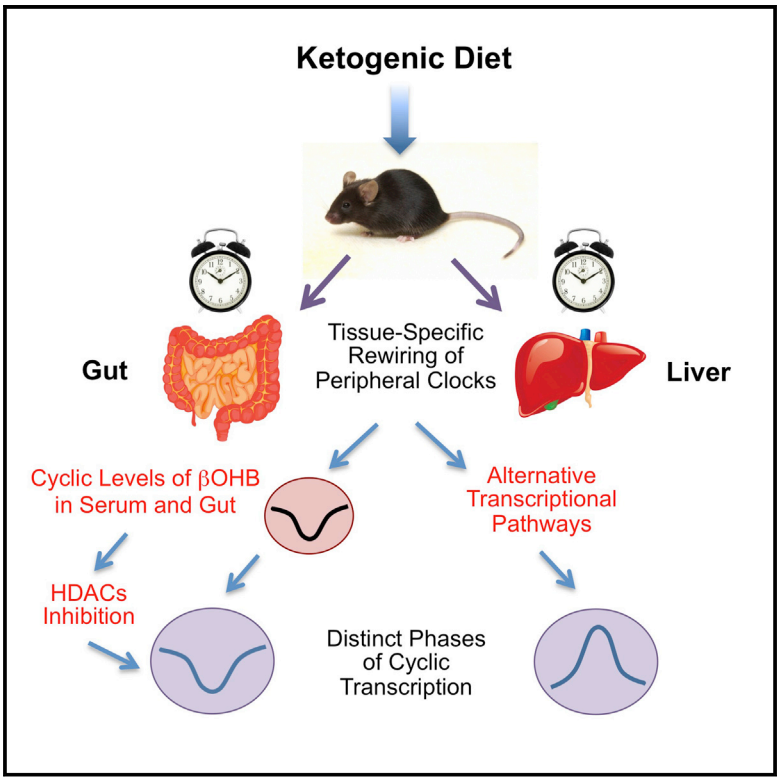

Authors

Paola Tognini, Mari Murakami, Yu Liu, ..., Eric Verdin, Pierre Baldi, Paolo Sassone-Corsi

Correspondence

psc@uci.edu

In Brief

Tognini et al. reveal how a ketogenic diet (KD) differently affects liver and intestine circadian clocks and drives tissue-specific oscillation of PPARα and its target genes. Serum and intestine βOHB shows a unique diurnal rhythmicity, associated with daily epigenetic changes exclusively in the gut.

Highlights

- KD induces tissue-specific reprogramming of the circadian clock in liver and gut
- KD induces an increase in liver BMAL1 chromatin recruitment and amplitude of CCGs
- KD drives tissue-specific oscillation of PPARα and its target genes
- Oscillation of βOHB in gut and serum parallels gut-specific cycling of H3 acetylation

Tognini et al., 2017, Cell Metabolism *26*, 523–538
September 5, 2017
http://dx.doi.org/10.1016/j.cmet.2017.08.015

Cell Metabolism
Article

Distinct Circadian Signatures in Liver and Gut Clocks Revealed by Ketogenic Diet

Paola Tognini,[1,5] Mari Murakami,[1,5] Yu Liu,[2,5] Kristin L. Eckel-Mahan,[1,3] John C. Newman,[4] Eric Verdin,[4] Pierre Baldi,[2] and Paolo Sassone-Corsi[1,6,*]

[1]Center for Epigenetics and Metabolism, Department of Biological Chemistry, U1233 INSERM
[2]Institute for Genomics and Bioinformatics, School of Information and Computer Sciences
University of California, Irvine, Irvine, CA, USA
[3]Center for Metabolic and Degenerative Diseases, Institute of Molecular Medicine, University of Texas Health Sciences Center, Houston, TX, USA
[4]Gladstone Institutes, University of California, San Francisco, 1650 Owens Street, San Francisco, CA 94158, USA
[5]These authors contributed equally
[6]Lead Contact
*Correspondence: psc@uci.edu
http://dx.doi.org/10.1016/j.cmet.2017.08.015

SUMMARY

The circadian clock orchestrates rhythms in physiology and behavior, allowing organismal adaptation to daily environmental changes. While food intake profoundly influences diurnal rhythms in the liver, how nutritional challenges are differentially interpreted by distinct tissue-specific clocks remains poorly explored. Ketogenic diet (KD) is considered to have metabolic and therapeutic value, though its impact on circadian homeostasis is virtually unknown. We show that KD has profound and differential effects on liver and intestine clocks. Specifically, the amplitude of clock-controlled genes and BMAL1 chromatin recruitment are drastically altered by KD in the liver, but not in the intestine. KD induces nuclear accumulation of PPARα in both tissues but with different circadian phase. Also, gut and liver clocks respond differently to carbohydrate supplementation to KD. Importantly, KD induces serum and intestinal β-hydroxyl-butyrate levels to robustly oscillate in a circadian manner, an event coupled to tissue-specific cyclic histone deacetylase (HDAC) activity and histone acetylation.

INTRODUCTION

The circadian clock is an endogenous timekeeper that provides organisms with the ability to anticipate daily fluctuations in the environment, thus allowing an appropriate physiological adaptation (Bass and Takahashi, 2010; Eckel-Mahan and Sassone-Corsi, 2013). The molecular clock is characterized by complex transcriptional-translational feedback loops involving both transcriptional activators and repressors. The positive limb of the mammalian clock machinery comprises CLOCK and BMAL1, which heterodimerize and induce the expression of clock-controlled genes (CCGs) by binding E-boxes on target promoters. Cryptochrome (*Cry1* and *Cry2*) and Period (*Per1*, *Per2*, and *Per3*) genes encode proteins that form the negative limb, inhibiting CLOCK:BMAL1-mediated transcription (Asher and Sassone-Corsi, 2015; Tamanini et al., 2007). Another important diurnal loop involves the transcriptional activator retinoid-related orphan receptors (RORs) and the repressor REV-ERBα/REV-ERBβ, which induces *Bmal1* rhythmic expression and delays *Cry1* expression (Everett and Lazar, 2014; Partch et al., 2014). A number of studies have shown that chromatin remodeling plays a central role in the harmonic oscillation of circadian gene expression (Koike et al., 2012). Among the chromatin remodelers linked to the molecular clock are the nuclear sirtuins, specifically SIRT1 (Asher et al., 2008; Nakahata et al., 2008) and SIRT6 (Masri et al., 2014). These are deacetylases that use NAD^+ as a co-enzyme, thus linking cellular energy metabolism with epigenetic control. Remarkably, SIRT1 activity and the levels of NAD^+ oscillate in a 24 hr manner since the molecular clock directly controls the circadian transcription of the gene encoding the enzyme nicotinamide phosphorybosiltransferase (NAMPT) (Nakahata et al., 2009; Ramsey et al., 2009). NAMPT operates as the rate-limiting step enzyme in the NAD-salvage pathway. Notably, NAD^+ oscillation is abolished in the liver under nutritional challenge by high-fat diet because of the lack of chromatin recruitment of the CLOCK:BMAL1 complex to the *Nampt* gene promoter (Eckel-Mahan et al., 2013).

The mammalian circadian system is a hierarchical network in which the central oscillator, located in the suprachiasmatic nuclei (SCN) of the hypothalamus, acts in concert with peripheral clocks (Mohawk et al., 2012; Okamura, 2004; Schibler and Sassone-Corsi, 2002). Importantly, both organismal and cellular metabolism are tightly interlocked with circadian rhythms and food challenges, such as high-fat diet or restricted feeding, that are able to profoundly remodel the liver circadian transcriptome and metabolome (Eckel-Mahan et al., 2013; Hatori et al., 2012; Kohsaka et al., 2007; Stokkan et al., 2001; Vollmers et al., 2009). The gut has a powerful endogenous clock that is thought to be implicated in time-specific food intake. The disruption of the clock causes higher risk of gut inflammation (Bellet et al., 2013; Tognini et al., 2017) and increased intestinal permeability (Summa et al., 2013). Interestingly, the crosstalk between gut microbiota and intestinal epithelial cells is mediated by the host clock, and clock impairment due to the absence of

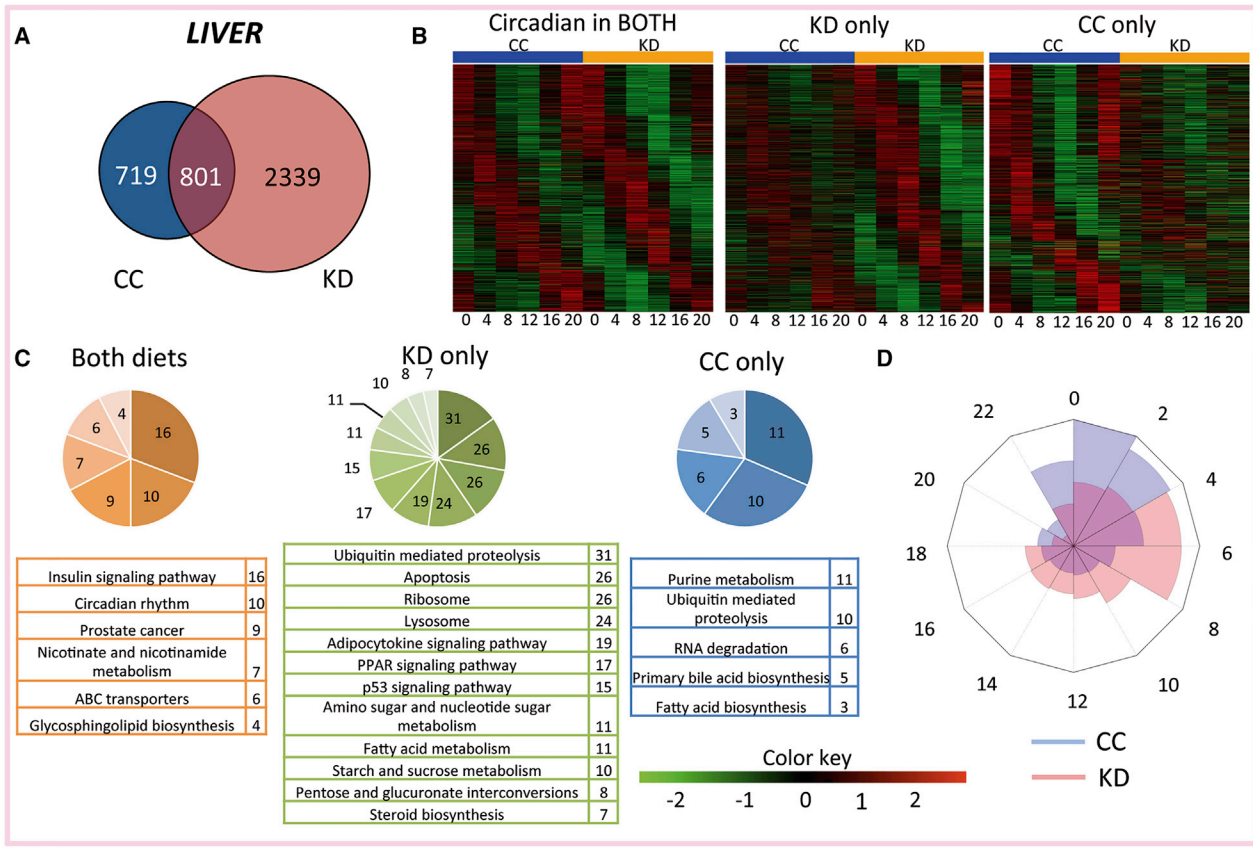

Insulin signaling pathway	16
Circadian rhythm	10
Prostate cancer	9
Nicotinate and nicotinamide metabolism	7
ABC transporters	6
Glycosphingolipid biosynthesis	4

Ubiquitin mediated proteolysis	31
Apoptosis	26
Ribosome	26
Lysosome	24
Adipocytokine signaling pathway	19
PPAR signaling pathway	17
p53 signaling pathway	15
Amino sugar and nucleotide sugar metabolism	11
Fatty acid metabolism	11
Starch and sucrose metabolism	10
Pentose and glucuronate interconversions	8
Steroid biosynthesis	7

Purine metabolism	11
Ubiquitin mediated proteolysis	10
RNA degradation	6
Primary bile acid biosynthesis	5
Fatty acid biosynthesis	3

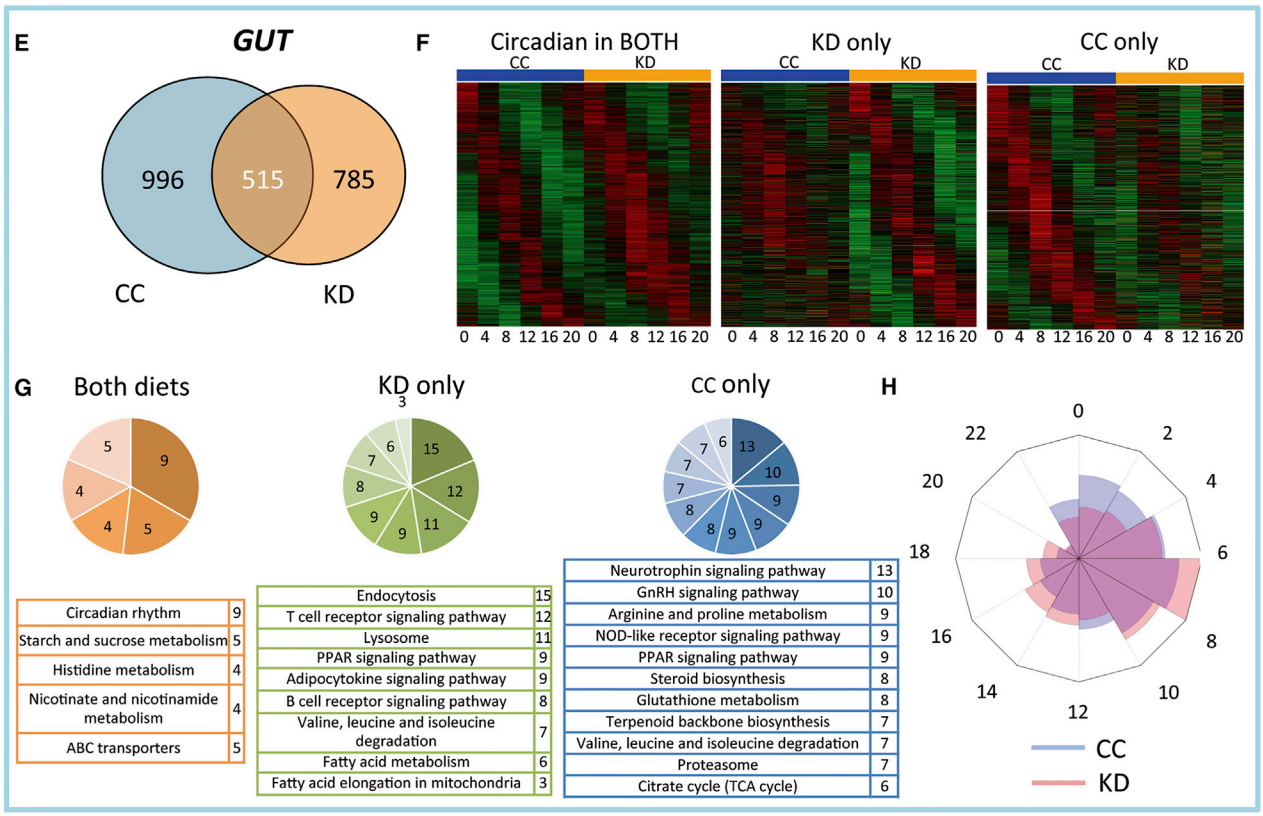

Circadian rhythm	9
Starch and sucrose metabolism	5
Histidine metabolism	4
Nicotinate and nicotinamide metabolism	4
ABC transporters	5

Endocytosis	15
T cell receptor signaling pathway	12
Lysosome	11
PPAR signaling pathway	9
Adipocytokine signaling pathway	9
B cell receptor signaling pathway	8
Valine, leucine and isoleucine degradation	7
Fatty acid metabolism	6
Fatty acid elongation in mitochondria	3

Neurotrophin signaling pathway	13
GnRH signaling pathway	10
Arginine and proline metabolism	9
NOD-like receptor signaling pathway	9
PPAR signaling pathway	9
Steroid biosynthesis	8
Glutathione metabolism	8
Terpenoid backbone biosynthesis	7
Valine, leucine and isoleucine degradation	7
Proteasome	7
Citrate cycle (TCA cycle)	6

(legend on next page)

microbial signaling induces a pre-diabetic status (Mukherji et al., 2013). In addition, food challenge-driven remodeling in the gut microbiota can transcriptionally rewire the liver clock (Leone et al., 2015; Murakami et al., 2016).

Both liver and intestine clocks play a key role in sustaining metabolic homeostasis. However, little is known about how the gut and liver clocks can specifically interpret a nutritional challenge and how diet variations might uniquely affect the circadian physiology of distinct peripheral organs. To address this conceptually critical question, we reasoned that the ketogenic diet (KD) would provide the unique opportunity to explore how specific diet-generated metabolites would differentially impact distinct peripheral clocks. Indeed, KD is a high-fat, adequate protein, very-low-carbohydrate diet that induces a switch to fatty acid oxidation as an energy source. The result is an overproduction of acetyl-CoA, which leads to the synthesis of ketone bodies via the activation of the ketogenic pathway. Ketone bodies refer to three distinct molecules, acetone, acetoacetic acid, and β- hydroxyl-butyrate (βOHB), that are produced principally in the mitochondrial matrix in the liver, during fasting or prolonged exercise (Hawley et al., 2014; Newman and Verdin, 2014). Mice fed a KD present a low level of glucose but increased blood level of βOHB, which is used as an energy source by the brain and other tissues (Douris et al., 2015; Kennedy et al., 2007). Interestingly, a central role for rhythmic release of βOHB from the liver appears to be implicated in driving food anticipation via feedback to the hypothalamus (Chavan et al., 2016). Furthermore, βOHB seems to function as a cofactor for a recently defined epigenetic mark, histone β-hydroxyl-butyrylation, involved in the control of gene expression under specific metabolic states (Xie et al., 2016).

Another relevant facet of KD is its use in therapeutics to treat refractory epilepsy in children as well as obesity and metabolic diseases. Moreover, KD has been under evaluation for alternative indications such as polycystic ovarian syndrome, cancer, and neurodegenerative diseases (Paoli et al., 2013). Despite this biomedical use, little is known about how KD impacts tissue-specific gene expression and how it may influence circadian homeostasis. Here we show that KD triggers distinct transcriptional responses by activating unique tissue-specific pathways involved in rewiring cyclic gene expression. Finally, we reveal that serum and intestinal βOHB levels display diurnal rhythmicity, which accompany a time-dependent HDAC activity and histone acetylation primarily in the gut. Our findings support the view that ketogenic-based nutrition contributes to diurnal transcriptional rewiring via metabolite-driven chromatin remodeling.

RESULTS

KD Abolishes Rhythmicity in Respiratory Metabolism

To explore how KD influences circadian physiology, we submitted 8-week-old C57BL/6 mice to KD dietary regimen during 4 weeks and compared them to control chow (CC)-fed mice. KD-fed mice lost weight in the first 2 weeks of the new dietary regimen and then stabilized to the same weight as CC-fed animals (Figure S1A), in line with previous studies (Kennedy et al., 2007). As expected, serum βOHB concentration significantly increased in KD-fed animals (Figure S1B). KD induced a significant decrease in serum glucose with respect to CC, although it remained in a physiological range (Figure S1C). To further understand the metabolic state induced by KD, animals were analyzed by indirect calorimetry for CO_2 emission, O_2 consumption, and energy intake. Notably, while the respiratory exchange ratio (RER) of normally fed mice oscillated along the circadian cycle, RER rhythmicity was abolished in KD-fed mice and remained flat throughout the circadian cycle with an average value of 0.7 (Figures S1D and S1E). This indicated that fat was the only fuel metabolized by KD-fed mice throughout the circadian cycle. Caloric and water intake (Figures S1F and S1G), as well as the feeding pattern (Figure S1F), were equivalent in CC- and KD-fed mice, showing that rhythmicity in food intake was not altered under KD.

Tissue-Specific Remodeling of Diurnal Transcription by KD

To gain further insight into how KD influences diurnal metabolism, we performed high-throughput profiling of hepatic tissue and ileal intestinal epithelial cells (IECs) by transcriptome microarrays. The analysis of rhythmic transcripts was performed using the non-parametric test JTK_CYCLE (Hughes et al., 2010), incorporating a window of 20–28 hr for the determination of circadian periodicity.

A first notable finding is that, while the number of cyclic genes in CC-fed mice was comparable between the liver and the gut, this ratio was drastically different in KD-fed mice, with a much larger number of genes oscillating in the liver (Figures 1A and 1E). Our analysis showed that 2,339 genes started to oscillate de novo in the liver upon KD, while cyclic transcripts under CC were 719. Genes displaying rhythmicity under both nutritional conditions were 801 in the liver (Figures 1A and 1B). Gene annotation analysis revealed specific categories for all groups (Figures 1C and S2A; Table S1). Remarkably, the effect of KD on the number of cycling transcripts in IECs was the opposite, with a decrease in oscillating genes (785, KD-only rhythmic

Figure 1. Heatmaps, KEGG Pathway, and Phase Lag Analyses of the Diurnal Transcriptome in Liver and Gut upon KD

(A) Venn diagram representing the number of genes rhythmic only in KD, only in CC, and in both conditions in the liver (n = 3 per time point, per group, $p < 0.01$, false discovery rate [FDR] < 0.1).

(B) Heatmaps representing the genes diurnal in both conditions, KD only, and CC only in liver (n = 3 per time point, per group, $p < 0.01$, FDR < 0.1).

(C) KEGG pathway analysis in liver. The numbers in the pie charts and tables represent the number of genes enriched in the specific KEGG pathway.

(D) Radar plots representing the phase lag of genes exclusively diurnal in KD or CC in hepatic tissue (Anderson-Darling test; phase distributions significance, $p < 0.0001$).

(E) Venn diagram representing the number of genes oscillating only in KD, only in CC, and in both conditions in the intestine (n = 3 per time point, per group, $p < 0.01$, FDR < 0.1).

(F) Heatmaps representing the genes diurnal in both conditions, KD only, and CC only in the gut (n = 3 per time point, per group, $p < 0.01$, FDR < 0.1).

(G) KEGG pathway analysis in the intestine. The numbers in the pie charts and tables represent the number of genes enriched in the specific KEGG pathway.

(H) Radar plots representing the phase lag of genes exclusively diurnal in KD or CC in ileal cells (Anderson-Darling test; phase distribution significance in IECs, KD versus CC, $p < 0.0001$; comparisons not shown; phase distribution difference upon KD, liver versus IECs, $p < 0.0001$; phase distribution difference upon CC, liver versus IECs, $p < 0.0001$).

transcripts) with respect to CC condition (996, CC-only rhythmic transcripts). Cyclic genes in both CC and KD in IECs were 515 (Figures 1E and 1F), and the most overrepresented Kyoto Encyclopedia of Genes and Genomes (KEGG) pathways among these genes, such as "circadian rhythm" and "nicotinate and nicotinamide metabolism," were the same of the liver "both" genes (Figures 1C, 1G, S2A, and S2B; Tables S1 and S2). The heatmaps of the oscillating transcripts showed the loss of rhythmicity in CC (Figures 1B and 1F, second map) and in KD (Figures 1B and 1F, third map). Disruption of diurnal oscillations in gene expression was particularly evident with an increased p value threshold ($p < 0.05$) in both liver (Figure S3A) and intestine (Figure S3B). For the complete list of genes oscillating in liver and IECs, see Tables S3 and S4.

It is worth noting that the transcripts rhythmic under either KD or CC (KD only and CC only) were enriched in a variety of different pathways in a tissue-specific manner (Figures 1C, 1G, S2A, and S2B; Tables S1 and S2), underscoring the unique metabolic states induced by KD in the gut and liver clocks.

To explore the physiological relevance of the diurnal alterations in the transcriptome under KD, we analyzed the levels of specific metabolites in the liver and intestine of KD-fed mice. Our KEGG pathway analysis indicated that "steroid biosynthesis" was a metabolic pathway circadian in KD-only liver (Table S1, sheet 2) and in CC-only IECs (Table S2, sheet 1). Indeed, we found a significant increase in total cholesterol levels in KD liver with respect to CC and a significant difference between zeitgeber time 0 (ZT0) and ZT12 (Figure 2A). On the other hand, we could not monitor convincing time-of-the-day-dependent changes in gut cholesterol levels or a significant difference between CC and KD (Figure 2C). The KEGG pathway analysis also indicated "fatty acid metabolism" as diurnal in both liver and IECs upon KD (Tables S1 and S2, sheet 2). In the liver, there was an increase in free fatty acid concentration upon KD, although no rhythmic alterations between the ZTs tested (Figure 2B). Strikingly, we found a strong increase in free fatty acid concentration in the gut at nighttime (ZT20), while in CC the levels were unchanged during night and day (Figure 2D). As fatty acids are ligands of the peroxisome proliferator-activated (PPAR) family of nuclear receptors (Grygiel-Górniak, 2014), these data nicely match the rhythmic nuclear accumulation of PPARα (Figure 4D) and its target gene expression (Figure 4E) in the intestine of mice fed to KD. In keeping with higher, but not diurnal, fatty acid levels, there was a non-circadian increase in the expression of PPARα target genes in the liver (Figure 4B) (see Cyclic Activation of PPARα by KD).

Interestingly, the KD-induced diurnal genes oscillated in a coordinated manner, in phase with a sharp peak at ZT6–ZT8 in the liver and ZT8 in the intestine, as shown by time lag analysis (Figures 1D and 1H). The genes oscillating in CC only were still coordinated in phase with an earlier peak around ZT2 in the liver and ZT8 in the gut (Figures 1D and 1H). Moreover, the amplitude analysis in "both diets" condition underlined another tissue-specific feature of the KD challenge: of all common oscillators, 54.7% of the 801 transcripts displayed an increase in amplitude in the liver upon KD feeding (Figure S2C). In contrast, in the gut 52% of the genes showed a decrease in amplitude and only 43% an increase (Figure S2D). Altogether, these data indicate that distinct diets control the phase and amplitude of oscillation of the circadian transcriptome via distinct mechanisms in different tissues.

To further determine the diurnal transcriptional signature induced by KD in the two distinct tissues, we analyzed the KD-driven rhythmic transcripts in liver and gut (Figure 2E; Table S5). The genes cycling exclusively upon KD in the liver were 2,724 and they clustered in the KEGG pathways "protein processing in endoplasmic reticulum," "TNF signaling pathway," and "glucagon signaling pathway" (see Table S6, sheet 1, for a complete list). Only 884 genes were rhythmic exclusively in the gut (Figure 2E) and they were prevalently enriched in "metabolic pathways"; "valine, leucine, and isoleucine degradation"; and "fatty acid degradation and elongation" (Table S6, sheet 2). The shared rhythmic genes were 416 and, as expected, comprised the core clock genes (Figure 2E; Table S6, sheet 3). The heatmaps of the oscillating transcripts showed a total disruption in diurnal rhythms of the exclusive cycling genes between the two tissues (Figure 2F), reinforcing the notion of transcriptional reprogramming in response to a food challenge of specific peripheral clocks (Eckel-Mahan et al., 2013).

Furthermore, to gain insight into the differential influence of KD on the liver and gut clock, transcription factor binding site (TFBS) enrichment analysis was performed based on MotifMap (Daily et al., 2011; Xie et al., 2009) binding site results (Table S6, sheet 4), and a further meta-analysis was used to identify tissue-specific rhythmic transcription factors (Figure 2G). Interestingly, *Pparα*, a nuclear receptor involved in ketogenic responses, was a transcription factor rhythmic in KD-only IECs (Figure 2G) and its binding motif was highly significant in genes rhythmic exclusively under this condition (Figure 2I). This suggested that the PPARα pathway could represent a specific diurnal signature in the KD-dependent rhythmic transcriptional rewiring of the gut clock. Other transcription factors displayed an oscillatory profile in the liver (Figure 2G) and some of the motifs bound by the STAT protein family were enriched in KD-only liver (Figure 2H). Importantly, "CLOCK:BMAL1" binding site was enriched in virtually all the conditions (Table S6, sheet 4) except for KD-only IECs when compared to KD-only liver. Moreover, "CLOCK:BMAL1" binding site was strongly significant in KD-only liver (Table S6, sheet 4; Figure 2H), implying a possible direct involvement of the core clock in interpreting a ketogenic nutritional challenge on hepatic tissue physiology.

Limited Effect of KD on Core Clock Gene Oscillation

The significant influence of KD on cyclic gene expression prompted us to determine whether it would directly affect the core clock machinery. To do so, we analyzed the expression of *Bmal1*, *Cry1*, *Per2*, and *Rev-erbα* genes and found no significant alteration in phase and amplitude when comparing CC- and KD-fed mice in both liver (Figure S3C) and IECs (Figure S3D). Moreover, BMAL1 protein and phosphorylation levels were virtually unaltered by KD as compared to CC in both liver (Figure S3E) and gut (Figure S3F) along the entire circadian cycle. Thus, core clock gene expression appears to be resistant to potential perturbations caused by a food challenge in two distinct peripheral clock systems.

Tissue-Specific Effect of KD on BMAL1 Chromatin Recruitment

Given the changes in gene cycling but subtle difference in core clock gene expression, we investigated other possible molecular mechanisms by which KD influences the diurnal transcriptional landscape. Therefore, we analyzed the expression profiles of

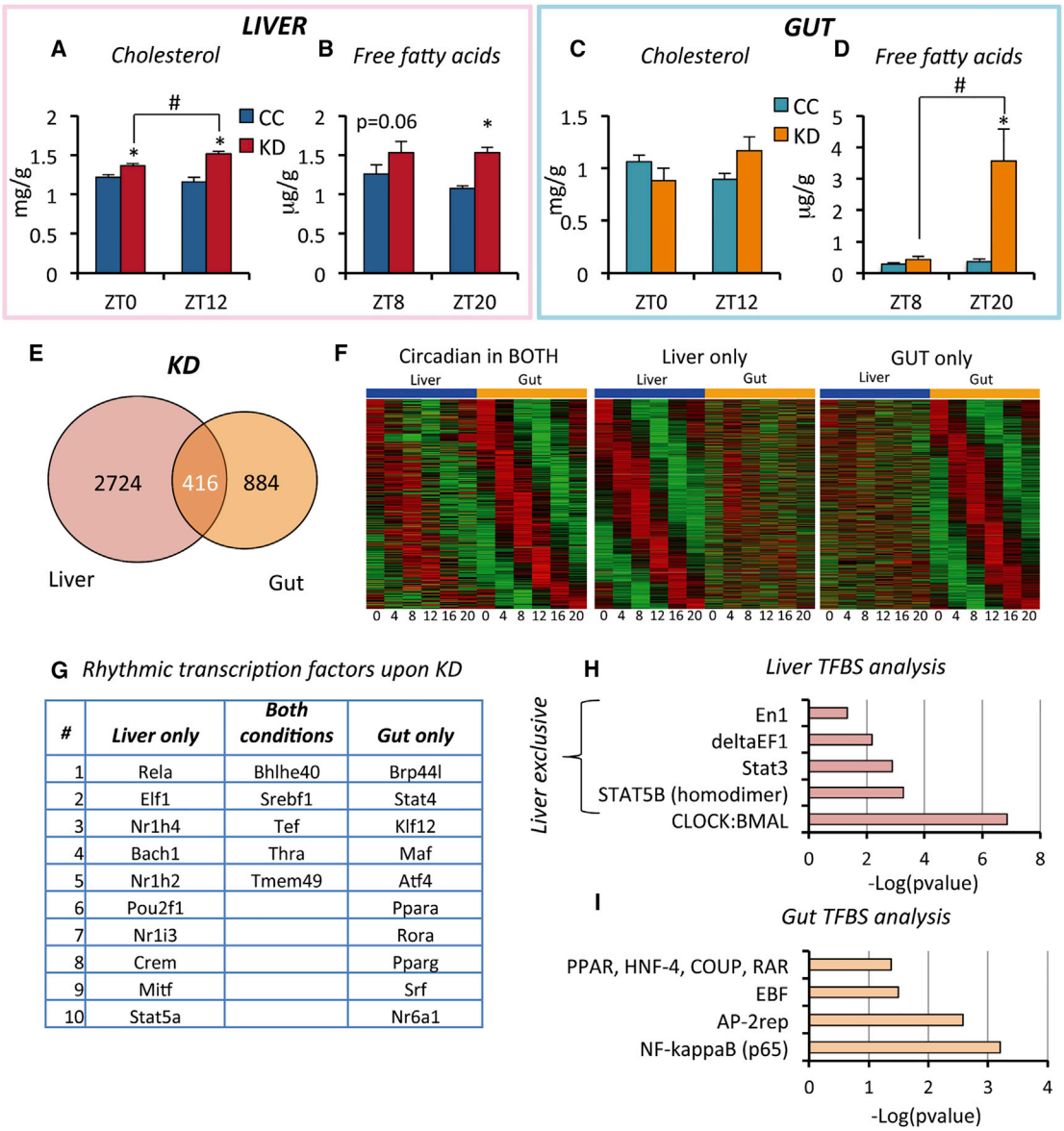

#	Liver only	Both conditions	Gut only
1	Rela	Bhlhe40	Brp44l
2	Elf1	Srebf1	Stat4
3	Nr1h4	Tef	Klf12
4	Bach1	Thra	Maf
5	Nr1h2	Tmem49	Atf4
6	Pou2f1		Ppara
7	Nr1i3		Rora
8	Crem		Pparg
9	Mitf		Srf
10	Stat5a		Nr6a1

Figure 2. Metabolite Levels and Circadian Transcriptional Signature in Liver versus IECs upon KD

(A) Hepatic total cholesterol levels at ZT0 and ZT12 in CC- and KD-fed mice (n = 4 per time point, per group; two-way ANOVA, Holm-Sidak post hoc; comparisons for factor, diet within ZT, *p < 0.05; ZT within KD, #p < 0.05).

(B) Free fatty acid levels in the liver of CC- and KD-fed mice at ZT8 and ZT20 (n = 4 per time point, per group; two-way ANOVA, Holm-Sidak post hoc; comparisons for factor, diet within ZT, *p < 0.05).

(C) Intestinal total cholesterol levels at ZT0 and ZT12 in CC- and KD-fed mice (n = 4 per time point, per group; two-way ANOVA, no significant difference).

(D) Free fatty acid levels in the ileum of CC- and KD-fed mice at ZT8 and ZT20 (n = 4 per time point, per group; two-way ANOVA, Holm-Sidak post hoc; comparisons for factor, diet within ZT, *p < 0.05; ZT within KD, #p < 0.05). Error bars represent SEM.

(E) Venn diagram representing the transcripts oscillating in "liver only," "both tissues," and "IECs only" upon KD feeding (n = 3 per time point, per group, p < 0.01, FDR < 0.1).

(F) Heatmaps representing the genes diurnal in both tissues, liver only, and intestine only upon KD (n = 3 per time point, per group, p < 0.01, FDR < 0.1).

(G) Analysis of the rhythmic transcription factors (p < 0.01) in animals fed KD, exclusively in the liver, in both tissues, or exclusively in the gut.

(H) Transcription factor binding site (TFBS) analysis in the liver of KD-fed mice. In the graph is reported the –log (pValue, 10). The first four sites are enriched exclusively in the liver upon KD. CLOCK:BMAL1 binding site is not exclusive, although it is highly enriched in KD liver, as shown by the value of the –log (pValue).

(I) Transcription factor binding site (TFBS) analysis in the IECs of KD-fed mice. In the graph is reported the –log (pValue, 10).

CCGs other than the core clock that, as previously mentioned, did not display any major alterations both in the liver and the gut (Figures S3C and S3D).

In the liver, KD induced a significant increase in the amplitude of CCG oscillation, such as *Dbp* (albumin D-box binding protein) and *Nampt* (nicotinamide phosphoribosyl transferase) (Figure 3A). The

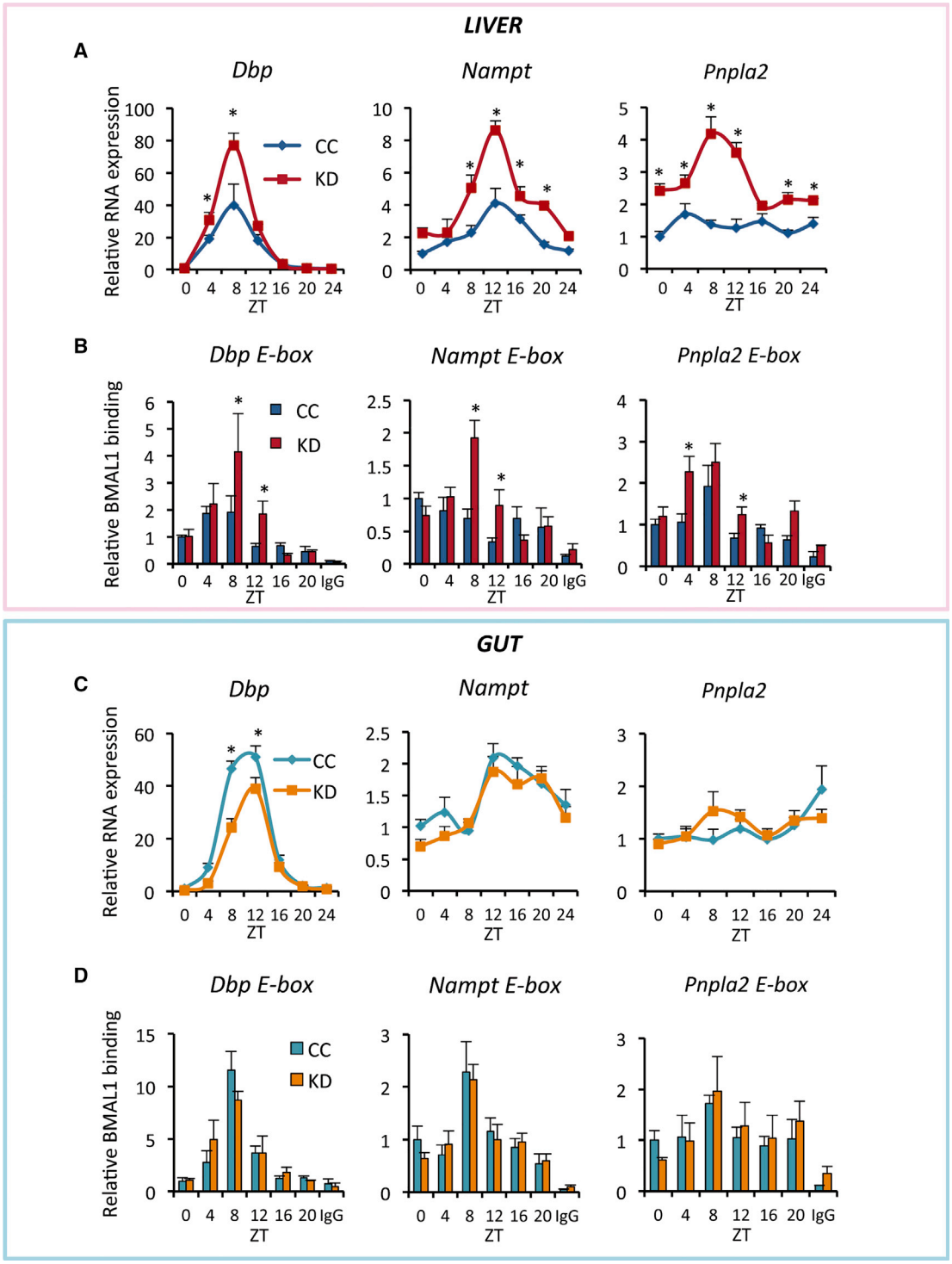

Figure 3. Clock-Controlled Gene Expression and BMAL1 Chromatin Recruitment on Specific Target Promoters

(A) Expression of clock output genes *Dbp*, *Nampt*, and *Pnpla2* measured by qPCR in the liver (n = 5 per time point, per group; two-way ANOVA, Holm-Sidak post hoc; comparisons for factor, diet within ZT, *p < 0.05).

(B) qPCR- ChIP results showing BMAL1 chromatin recruitment on the E-boxes of the *Dbp*, *Nampt*, and *Pnpla2* gene promoters in the liver (n = 5 per time point, per group; two-way ANOVA, Holm-Sidak post hoc; comparisons for factor, diet within ZT, *p < 0.05).

(C) Expression of clock output genes *Dbp*, *Nampt*, and *Pnpla2* measured by qPCR in IECs (n = 5 per time point, per group; two-way ANOVA, Holm-Sidak post hoc; comparisons for factor, diet within ZT, *p < 0.05).

(legend continued on next page)

example of *Nampt* is notable since, in contrast to KD, its circadian expression is completely abolished by high-fat diet in the liver (Eckel-Mahan et al., 2013). The profile of *Pnpla2* (patatin-like phospholipase domain containing 2, also known as *Atgl*), a rhythmic gene involved in lipid metabolism, was also altered (Figure 3A), displaying a significant amplitude enhancement in the liver (Figure 3A). In the gut, the effect of KD on these genes was drastically different. In fact, the expression of *Dbp*, *Nampt*, and *Pnpla2* was virtually identical to the profile under CC (Figure 3C). Importantly, there was no increase of *Nampt* and *Pnpla2* gene expression at ZT12 upon KD in *Clock*-deficient mice, both in liver and intestine (Figures S3G and S3H). This result indicates that a functional clock is required to mediate the effect of KD on hepatic rhythmic transcriptional changes.

To decipher the molecular mechanism responsible for the enhancement in CCG amplitude, we performed chromatin immunoprecipitation (ChIP) experiments using BMAL1 antibodies. Strikingly, BMAL1 recruitment on the E-boxes within *Dbp* and *Nampt* promoter regions was significantly increased at ZT8 and ZT12, and at ZT4 and ZT12 on *Pnpla2* E-box in the liver of KD-fed animals (Figure 3B). In contrast, BMAL1 binding to the E-boxes of the same genes showed no differences in the IECs (Figure 3D). In line with these results, cross-analysis of our diurnal transcriptome with BMAL1 ChIP sequencing (ChIP-seq) data (Koike et al., 2012; Rey et al., 2011) indicated that the majority of cyclic BMAL1 targets in the liver of KD-fed mice had a robust peak at ZT8 (Figure S4A) and an increase in their expression at the same ZT with respect to CC-fed mice (Figure S4E). Similarly, other clock output genes, such as *Nmnat3* and *Bhlhe41*, displayed a significant enhancement in their oscillation with a zenith at ZT8 (Figures S4G and S4H), accompanied by a significant increase in BMAL1 chromatin recruitment on their promoters upon KD feeding (Figures S4G and S4H). In contrast, no changes in BMAL1 binding were observed at the E-boxes on *Per2* and *Rev-erbα* promoters (Figure S4I), perfectly correlating with no major alterations in core clock gene transcription in KD liver (Figure S3C). On the other hand, BMAL1 target genes displayed no increase in their level under KD in the gut (Figures S4B and S4F). Moreover, the phase-lag analysis of BMAL1 target cyclic genes showed a different pattern in the peak and nadir between liver and gut both for CC- or KD-fed animals (Figures S4C and S4D). Thus, while the global levels of BMAL1 protein seem to be unaffected by KD feeding, BMAL1 chromatin recruitment to specific targets appears to be a critical control step in the liver of KD-fed mice. It is worth noting that these results are in keeping with the TFBS analysis, in which the "CLOCK:BMAL1" motif was highly enriched in the rhythmic liver transcriptome of KD-fed mice (Figure 2H; Table S6, sheet 4).

Taken together, these data show that KD modulates specific CCG oscillation by influencing the chromatin recruitment of the endogenous clock complex in the liver, but not in the gut. Thus, our findings underlie a tissue-dependent effect on clock protein functions upon a nutritional challenge.

Cyclic Activation of PPARα by KD

A central pathway highly enriched in our high-throughput genomic analysis is "PPAR signaling," clustered in the class of genes oscillating in "KD-only" in both liver and intestine (Figures 1C and 1G). It is worth noting that this GO category was present also in "CC-only" cycling genes in the gut, although the significance of the cluster in "CC-only" is much lower than in "KD-only" (Figure S2B). Moreover, the PPAR binding motif was significantly enriched in KD-only IECs (Figure 2I). Importantly, PPARα-driven transcription is implicated in the metabolic response to energy deprivation (Kersten et al., 1999). Furthermore, PPARα is a key regulator of lipid metabolic homeostasis and a prime mediator of ketogenesis (Badman et al., 2007; Leone et al., 1999). Thus, we examined the possible role of PPARα in the KD-induced cyclic transcriptional reprogramming in liver and gut. Importantly, PPARα nuclear protein levels were robustly upregulated upon KD in both liver and gut (Figures 4A and 4D). Daily oscillations of nuclear PPARα protein expression in KD-fed animals were anti-phasic in the two tissues, with a peak at around ZT8 in the liver and a trough at the same ZT in the gut (Figures 4A and 4D). Remarkably, PPARα target genes in the liver (Figure 4B) had a distinct profile with respect to the cyclic profile of the corresponding genes in the gut (Figure 4E), following the nuclear accumulation of PPARα in the two tissues (Figures 4A and 4D). Notably, PPARα targets *Hmgcs2* (3-hydroxy-3-methylglutaryl-CoA synthase 2), the rate limiting enzyme of the ketogenic pathway; *Acot2* (acyl-CoA thioesterase 2); *Angptl4* (angiopoietin-like 4); and *Cpt1a* (carnitine palmitoyltransferase 1A) robustly oscillate in IECs (Figure 4E) in phase with PPARα nuclear protein abundance (Figure 4D) and following the mouse feeding rhythm. It is worth noting that *Hmgcs2* exhibited a robust gain in oscillation in IECs, showing an increase of more than 25-fold compared to CC at the peak time point (Figure 4E). On the other hand, not all the liver PPARα targets displayed a clear rhythmic oscillation (Figure 4B). For example, hepatic *Hmgcs2* was only moderately increased during the daily ZTs, despite the significant upregulation in βOHB in KD-fed mice (Figure S1B). It is conceivable that HMGCS2 activity may be mainly regulated by post-translational modifications, in keeping with previously reported findings (Rardin et al., 2013; Shimazu et al., 2010). *Acot2* was significantly upregulated in KD-fed mice at all times of the circadian cycle, although it did not present a clear rhythmic behavior. Finally, hepatic *Cpt1a* and *Angptl4* exhibited a significant expression increase and gain in the amplitude of oscillation (Figure 4B).

To gain further insight into the cyclic activation of the PPARα pathway upon KD, we analyzed the daily expression of known PPARα target genes (Rakhshandehroo et al., 2010). The major biological pathways in which PPARα targets are involved are presented as a pie chart (Figure S5A). Strikingly, in the gut ~20% of these genes oscillated in phase with PPARα nuclear accumulation, as shown by the heatmap (Figure S5B, see the arrow). Thereby, it appears that the KD is imposing a stricter phase of oscillation for a number of genes in the gut. The majority of

(D) ChIP results showing BMAL1 chromatin recruitment on the E-boxes of *Dbp*, *Nampt*, and *Pnpla2* gene promoters in IECs (n = 5 per time point, per group; two-way ANOVA, Holm-Sidak post hoc; comparisons for factor, diet within ZT, no significant difference).
IgG represents ChIP experiment performed with an isotype-matched control immunoglobulin (normal rabbit IgG) to BMAL1.
Error bars represent SEM.

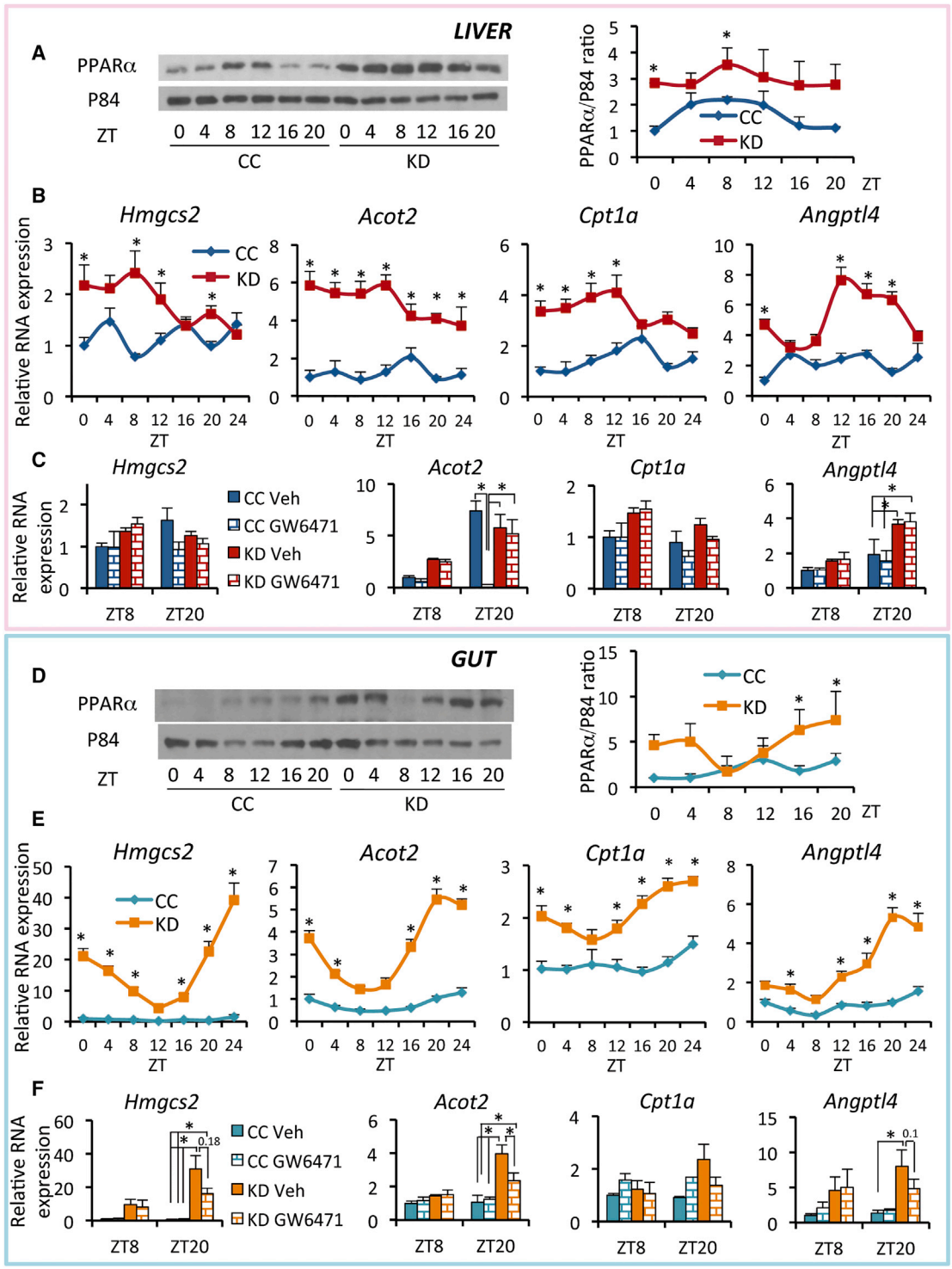

Figure 4. Tissue-Specific Circadian PPARα Signature in Liver and Intestine upon KD

(A) Western blot analysis of PPARα in liver nuclear extract. On the left, representative blot; on the right, graph reporting the average of the blot band density (n = 3 per time point, per group; two-way ANOVA, Holm-Sidak post hoc; comparisons for factor, diet within ZT, *p < 0.05).

(B) Expression of the PPARα target genes *Hmgcs2*, *Acot2*, *Cpt1a*, and *Angptl4* in liver extract (n = 5 per time point, per group; two-way ANOVA, Holm-Sidak post hoc; comparisons for factor, diet within ZT, *p < 0.05).

(C) Liver PPARα target gene expression in mice fed CC or KD for 4 weeks and treated with the specific PPARα inhibitor GW6471 (n = 3–4 per time point, per group; two-way ANOVA, Holm-Sidak post hoc; comparisons for factor, diet within ZT, *p < 0.05).

(legend continued on next page)

these targets participated in specific metabolic pathways such as "mitochondrial β-oxidation/oxidative phosphorylation" and "peroxisomal β-oxidation." In contrast, the same genes in the liver were not rhythmic and their profile was completely different with respect to the one in IECs (Figure S5C), as already indicated by the qPCR data (Figure 4B). Importantly, treatment of CC- or KD-fed mice with the specific PPARα inhibitor GW6471 influenced PPARα target gene levels at ZT20, the peak time point in KD-fed mice, in the ileum (Figure 4F), but not in the liver (Figure 4C).

Therefore, our results show that KD activates a tissue-specific rhythmic PPARα-dependent transcriptional reprogramming characterized by a well-defined phase of oscillation exclusively in the intestine, which differs from the liver.

KD Induces Circadian βOHB Levels and Rhythmic Histone Acetylation in the Gut

To determine the molecular mechanisms contributing to the different diurnal expression of PPARα targets in liver and intestine, we monitored the abundance of acetyl-(Lys9/Lys14) on histone H3 at PPRE (PPAR response element) sites on target promoters. The levels of acetylated H3 followed the daily transcriptional changes in IECs of KD-fed animals, with a higher increase at ZT20 than at ZT8 for all tested promoters (*Hmgcs2-PPRE*, *Acot2-PPRE*, *Cpt1a-PPRE*, and *Angptl4-PPRE*; Figure 5B). In keeping with PPARα targets profile, no significant changes in the rhythmicity of acetyl-(Lys9/Lys14) could be observed in the liver (Figure 5A). Strikingly, there was a robust oscillation of βOHB serum levels along the diurnal cycle in KD-fed mice, peaking at ZT0–ZT20 and reaching nadir at ZT8 (Figure 5C), with a diurnal profile mirroring the one of PPARα nuclear accumulation and PPARα target expression in the intestine (Figures 4D and 4E). Indeed, cyclic expression of ileal *Hmgcs2* may partially be responsible for the daily profile of βOHB levels. As βOHB is an endogenous histone deacetylase inhibitor (Shimazu et al., 2013), we reasoned that cyclic βOHB might generate rhythmicity in HDAC activity contributing to de novo oscillation of PPARα target genes. To explore this possibility, we analyzed HDAC activity in nuclear extract from intestine during daytime (ZT8) and nighttime (ZT20). We found that HDAC activity displayed an opposite profile with respect to serum βOHB oscillation in KD gut, being higher at ZT8 and lower at ZT20 (Figure 5G). Moreover, HDAC activity was significantly decreased in the gut of KD-fed mice as compared to CC-fed mice at ZT20 (Figure 5G), in line with the increase in histone H3 acetylation at specific promoter regions (Figure 5B). HDAC activity in nuclear extracts from CC-fed mice was virtually identical at ZT8 and ZT20, in keeping with the lack of βOHB rhythmicity (Figure 5C) and H3 acetyl-(Lys9/Lys14) in CC-fed mice (Figure 5B). Notably, the local concentration of βOHB in KD intestine remarkably mirrored the diurnal profile of the same metabolite in the serum (Figure 5E), strongly supporting the inhibitory effect on HDAC activity and the time-of-the-day-dependent changes in histone acetylation in this specific tissue. On the other hand, βOHB levels in the liver of KD-fed animals were still increased, although displaying a different oscillatory pattern with a peak at ZT12–ZT16 (Figure 5D). Furthermore, hepatic HDAC activity did not show any significant difference between CC and KD and only a negligible day-night difference (Figure 5F). To rule out the possibility that HDAC inhibition may occur at a diverse ZT in the liver, we monitored the abundance of acetyl-(Lys9/Lys14) on histone H3 on the same promoter regions (*Hmgcs2-PPRE*, *Acot2-PPRE*, *Cpt1a-PPRE*, and *Angptl4-PPRE*) at ZT0 and ZT12, the nadir and zenith, respectively, of the local hepatic βOHB. No changes were observed on H3 acetylation between CC and KD conditions or between the two ZTs analyzed (Figure S4J).

To demonstrate the direct link between βOHB, gene expression, and changes in histone acetylation in the gut, mice were fed CC or a diet corresponding to CC containing 10% (w/w) 1,3-butanediol (1,3 butanediol diet, BD) for 4 weeks. This is a strategy to increase the endogenous βOHB levels without inducing the metabolic state characteristic of a KD (Hashim and VanItallie, 2014). 1,3-butanediol is an alcohol precursor of βOHB and it is quickly converted to βOHB in the liver by the alcohol dehydrogenase system (Veech, 2014). As expected, βOHB serum concentration was significantly increased both at ZT8 and ZT20 upon BD (Figure S6A). PPARα target gene expression in the liver did not show any substantial difference after 4 weeks of BD (Figure S6B), as predicted because 1,3-butanediol does not involve any aspect of fatty acid metabolism. In keeping with this observation, only marginal changes in H3 acetyl-(Lys9/Lys14) on the promoter of the same genes were detected (Figure S6C). Notably, a significant upregulation in PPARα target genes was present in the intestine of BD-fed mice (Figure S6D). Interestingly, H3 acetyl-(Lys9/Lys14) abundance on the promoter region of *Acot2*, *Cpt1a*, and *Angptl4* was higher upon BD (Figure S6E), paralleling gene expression and reinforcing our hypothesis that βOHB specifically impacts this type of histone post-translational modification in the gut. Taken together, our results unveil a novel and tissue-specific epigenetic role of βOHB in rewiring cyclic gene expression upon a nutritional challenge.

Sucrose and Fructose Complementation of KD

As KD is devoid of carbohydrates, we questioned whether complementation with either fructose or sucrose would influence the metabolic effect of KD on the diurnal program. Carbohydrates have been shown to inhibit the induction of ketogenesis (Fukao et al., 2004). To do so, KD- or CC-fed mice were subjected to oral gavage with fructose (4 g/kg of body weight) for 7 days once a day, during the last week of their dietary regimen. Tissues were collected at ZT0 and ZT12, respectively the end

(D) Nuclear PPARα protein accumulation in IECs. On the left, representative blot; on the right, graph reporting the average of the blot band density (n = 3 per time point, per group; two-way ANOVA, Holm-Sidak post hoc; comparisons for factor, diet within ZT, *p < 0.05).
(E) PPARα target gene expression of *Hmgcs2*, *Acot2*, *Cpt1a*, and *Angptl4* in IECs (n = 5 per time point, per group; two-way ANOVA, Holm-Sidak post hoc; comparisons for factor, diet within ZT, *p < 0.05).
(F) Ileum PPARα target gene expression in mice fed CC or KD for 4 weeks and treated with the specific PPARα inhibitor GW6471 (n = 3–4 per time point, per group; two-way ANOVA, Holm-Sidak post hoc; comparisons for factor, diet within ZT, *p < 0.05).
Error bars represent SEM.

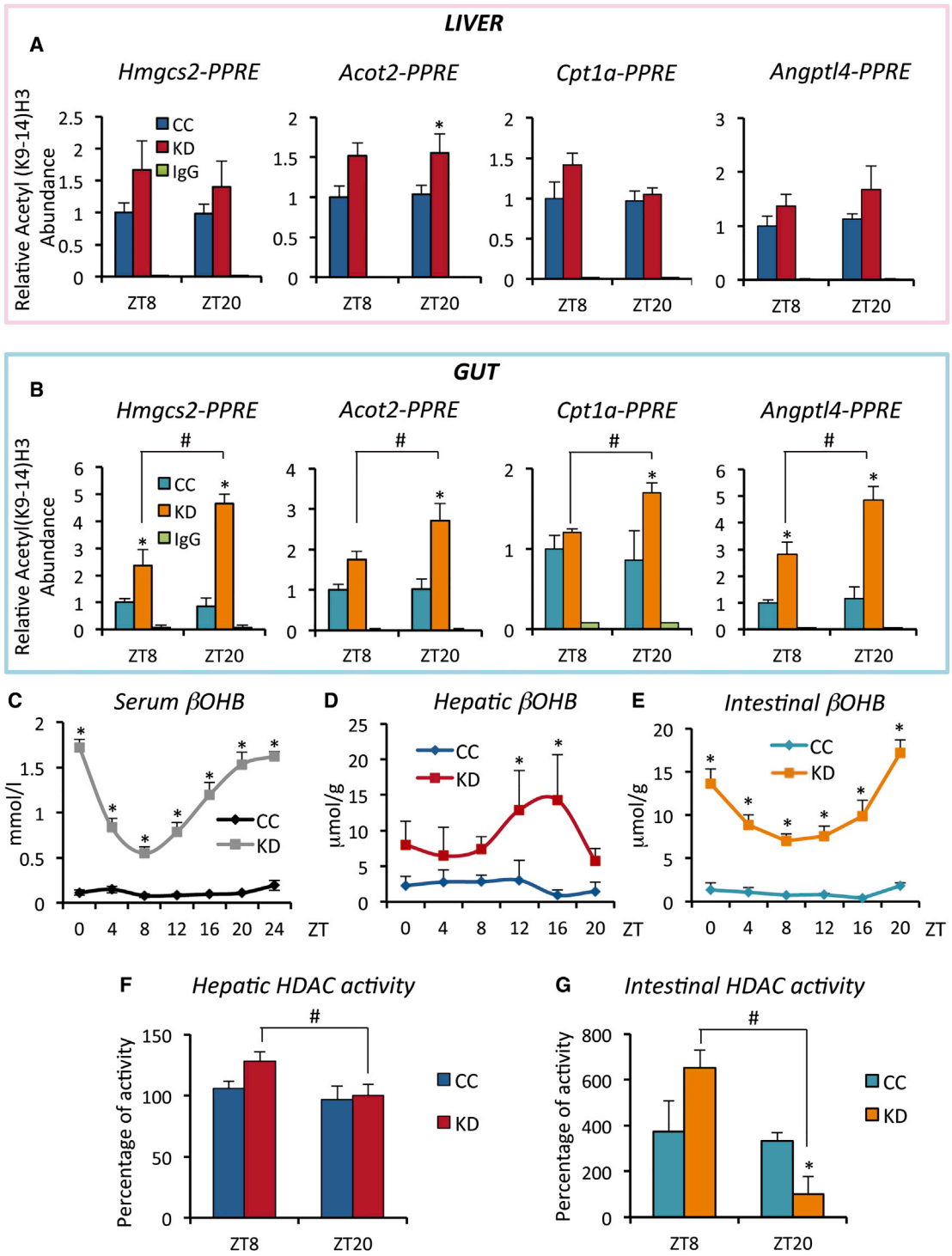

Figure 5. KD-Driven Oscillation in Serum βOHB and Daily Changes in Epigenetic Marks

(A) Liver ChIP of acetylated (Acetyl) lysine (K) 9-14 on histone H3. qPCR showing the relative abundance of H3 Acetyl(K9-K14) on the PPAR-responsive element (PPRE) of specific promoter: *Hmgcs2*, *Acot2*, *Cpt1a*, and *Angptl4* (n = 4–6 per time point, per group; two-way ANOVA, Holm-Sidak post hoc; comparisons for factor, diet within ZT, *p < 0.05).

(B) H3 Acetyl(K9-K14) abundance on the PPRE of *Hmgcs2*, *Acot2*, *Cpt1a*, and *Angptl4* promoter in the intestine (n = 4 per time point, per group; two-way ANOVA, Holm-Sidak post hoc; comparisons for factor, diet within ZT, *p < 0.05; ZT within KD, #p < 0.05).

(C) Serum βOHB levels along the diurnal cycle in CC- and KD-fed mice (n = 5 per time point, per group; two-way ANOVA, Holm-Sidak post hoc; comparisons for factor, diet within ZT, *p < 0.05).

(legend continued on next page)

and the beginning of the active phase. We focused our attention on a set of genes involved in KD metabolic response both in hepatic and ileal tissues. No significant effect of fructose was noted in the liver of KD-fed mice on *Hmgcs2*, *Acot2*, and *Angptl4* gene expression (Figure 6A). In sharp contrast, fructose induced a significant reduction in the expression of all these transcripts in the intestine (Figure 6C). Moreover, core clock genes and CCGs were only marginally influenced by fructose supplementation both in the liver (Figure S7A) and in the gut (Figure S7C). Thus, clock effects in the liver may be due to altered upstream signaling pathways that are selectively recruited over time to adapt to the change in fuel availability and drive downstream circadian events in a tissue-specific manner.

To test the effect of sucrose administration on KD-induced clock response, CC- or KD-fed mice were treated with 30% sucrose in drinking water for all 4 weeks of diet. Concomitant sucrose administration was insufficient to alter KD-specific clock response in the liver as only the expression of *Acot2* was moderately affected (Figure 6B). In contrast, the intestinal clock was robustly responsive to sucrose administration with an almost complete reversal of KD-induced metabolic changes. Indeed, gene expression of all the tested genes (*Hmgcs2*, *Acot2*, and *Angptl4*) returned to the levels distinctive of CC-fed mice (Figure 6D). Interestingly, sucrose did not interfere with core clock genes and CCGs in the liver of KD-fed mice, although it significantly influenced gene expression in CC-fed mice (Figure S7B), suggesting that KD could reinforce the core clock robustness in the liver. Similarly, sucrose affected core clock gene expression in the gut of CC-fed mice, although it also impacted CCG levels upon KD (Figure S7D).

Thus, in contrast to the liver, the intestinal clock exhibits a rapid response to carbohydrates that leads to increased plasticity in transcriptional reprogramming, further underlying the distinct and tissue-specific response of peripheral clocks upon dietary perturbation.

DISCUSSION

Metabolic homeostasis is connected to circadian function and both central and peripheral clocks contribute to its maintenance. The liver clock has been extensively studied because of its role in metabolic regulation. The intestinal clock, although obviously of importance, has been less investigated despite its central involvement in sustaining organismal metabolic responses (Mukherji et al., 2013). For the first time, we have questioned how two different tissues would operate their intrinsic, specialized plasticity to respond to a distinct nutritional challenge. We reveal a tissue-specific cyclic signature in response to a KD regimen that leads to a dramatic increase in β-oxidation and consequent ketosis (Paoli et al., 2015). While the impact of KD on the circadian clock has been noted (Genzer et al., 2015; Oishi et al., 2009), the molecular mechanisms underlying its action have not been satisfactorily explored. Our study represents the first exhaustive analysis of how KD influences rhythmic genomic reprogramming. In addition, as KD has been extensively used for the treatment of refractory epilepsy in children and for many other applications in adults such as obesity, diabetes, neurodegenerative disorders, and cancer (Paoli et al., 2013), our findings may provide a framework for future explorations of how circadian control could contribute to these pathophysiological conditions.

One of the most interesting properties of KD is its ability to drive metabolic pathways generally induced by fasting or caloric restriction. In fact, gluconeogenesis, fatty acid oxidation, and ketogenesis are upregulated while glycolysis and de novo lipogenesis are shut down (Kennedy et al., 2007; Paoli et al., 2015). Interestingly, enzymes and transcription factors involved in these metabolic cascades display circadian rhythmicity or start to oscillate upon KD, underscoring the tight link with the circadian clock. Our results show that KD is able to modulate the clock machinery recruitment to chromatin, which led to gain in oscillation of CCGs in the liver. Despite a very high fat content in KD, this effect was the opposite of a high-fat diet, which hindered BMAL1 chromatin recruitment to target genes (Eckel-Mahan et al., 2013), opening new questions about how nutrient composition can modulate the core clock-chromatin interaction. Here we report a significant increase in BMAL1 binding on *Nampt* and *Dbp* promoters both at ZT8 and ZT12, and at ZT4 and ZT12 on *Pnpla2* promoter, that results in a robust increase in their amplitude. Intriguingly, crossing our diurnal microarray data with BMAL1 ChIP-seq unveiled that BMAL1 target genes cycling in KD liver displayed a robust peak at ZT8. Taken together, these data suggest that KD-driven BMAL1 chromatin recruitment participates in the regulation of systemic adaptive responses to KD. On the other hand, the gut core clock was not affected by KD, indicating that the core clock machinery contributes to the physiological adaptation to a KD challenge in a tissue-specific manner, crosstalking directly with the metabolic clock exclusively in the liver.

The robust PPARα signaling activation induced in the gut of KD-fed mice paralleled the mouse food intake, suggesting that daily changes in PPARα signaling were primarily mediated by local physiological responses to feeding behavior rather than alterations in the core clock machinery. Indeed, the intestinal local levels of free fatty acids were remarkably increased at ZT20 with respect to ZT8 upon KD, respectively the peak and trough of PPARα nuclear concentration and its target gene expression (Figures 4D and 4E). Intriguingly, although PPARα pathway was induced both in liver and gut during ketogenesis, the two tissues displayed different phase of oscillation in both PPARα

(D) Hepatic βOHB levels along the diurnal cycle in CC- and KD-fed mice (n = 3 per time point, per group; two-way ANOVA, Holm-Sidak post hoc; comparisons for factor, diet within ZT, *p < 0.05).
(E) Intestinal βOHB levels along the diurnal cycle in CC- and KD-fed mice (n = 3 per time point, per group; two-way ANOVA, Holm-Sidak post hoc; comparisons for factor, diet within ZT, *p < 0.05).
(F) HDAC activity from liver nuclear extract at ZT8 and ZT20 (n = 5 per time point, per group; two-way ANOVA, Holm-Sidak post hoc; comparisons for factor, diet within ZT, no significant difference; ZT within KD, #p < 0.05).
(G) HDAC activity in intestinal nuclear extract at ZT8 and ZT20 (n = 3–5 per time point, per group; two-way ANOVA, Holm-Sidak post hoc; comparisons for factor, diet within ZT, *p < 0.05; ZT within KD, #p < 0.05).
Error bars represent SEM.

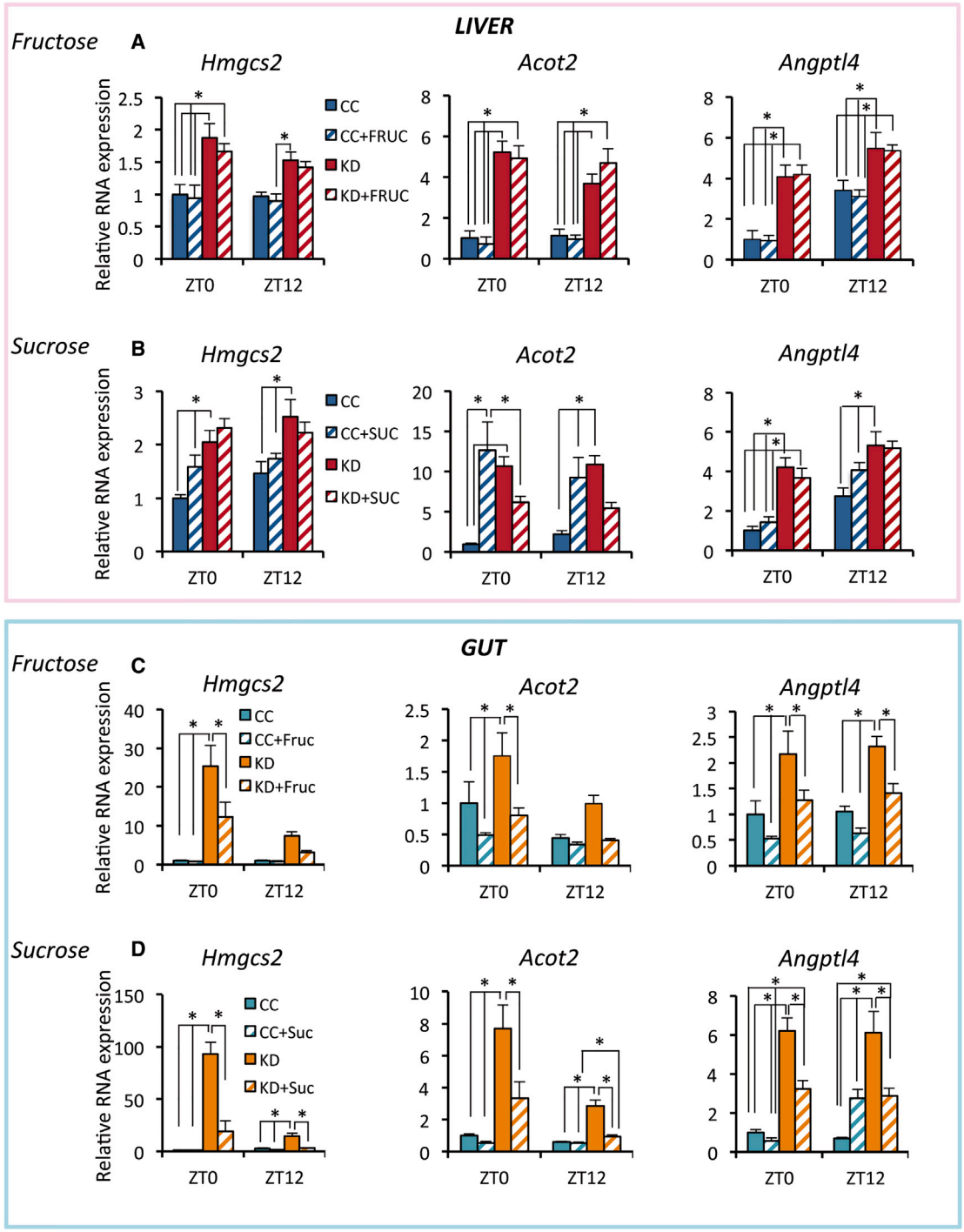

Figure 6. Liver and Intestine Response to Perturbation in Diet Composition

(A) qPCR of genes involved in the ketogenic response, *Hmgcs2*, *Acot2*, and *Angptl4*, in the liver of mice fed 4-week KD or CC and administered with fructose oral gavage (4 g/Kg) once a day, per 7 days during the last week of dietary regimen (n = 5–6 per time point, per group; two-way ANOVA, Holm-Sidak post hoc; comparisons for factor, diet within ZT, *p < 0.05).

(B) *Hmgcs2*, *Acot2*, and *Angptl4* gene expression in the liver of animals fed 4-week KD or CC and simultaneously treated with 30% sucrose in the drinking water (n = 5 per time point, per group; two-way ANOVA, Holm-Sidak post hoc; comparisons for factor, diet within ZT, *p < 0.05).

(C) Intestinal gene expression of *Hmgcs2*, *Acot2*, and *Angptl4* in mice subjected to fructose oral gavage (n = 5–6 per time point, per group; two-way ANOVA, Holm-Sidak post hoc; comparisons for factor, diet within ZT, *p < 0.05).

(D) qPCR analysis of *Hmgcs2*, *Acot2*, and *Angptl4* genes in the intestine of animals treated with 30% sucrose in the drinking water (n = 5 per time point, per group; two-way ANOVA, Holm-Sidak post hoc; comparisons for factor, diet within ZT, *p < 0.05).

Error bars represent SEM.

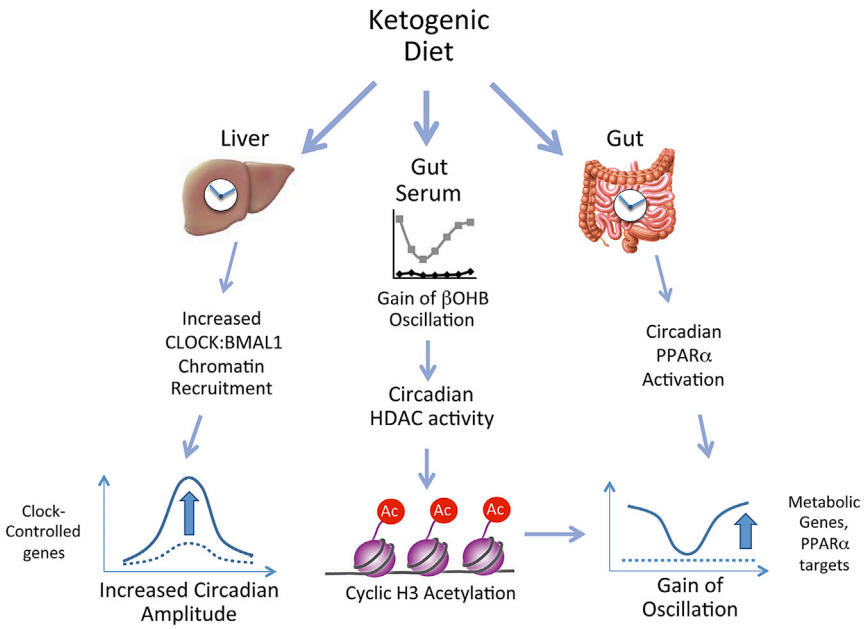

Figure 7. Schematic Representation of KD-Dependent Diurnal Signature in Liver and Intestine

A very-low-carbohydrate KD is able to reprogram peripheral clocks in liver and intestine through the activation of distinct transcription factors in a diurnal manner. KD enhances BMAL1 chromatin recruitment in the liver, resulting in an increase in the amplitude of oscillation of CCGs. KD activates the PPARα pathway both in liver and intestine but is highly diurnal only in the gut. The activation of ketogenesis increases serum βOHB concentration that oscillates in a diurnal fashion. Through circulation, βOHB is distributed to all the tissues as an energy source. The effect of βOHB is primarily evident in the intestine, where the metabolite oscillates with the same phase of serum βOHB, and it leads to regulated HDAC activity in a time-of-the-day-dependent fashion. This results in the increase of histone H3 acetylation on metabolic gene promoters at specific ZTs, contributing to rhythmic gene expression. Indeed, PPARα targets display a unique diurnal profile that nicely parallels PPARα nuclear accumulation and serum/intestinal βOHB daily changes.

nuclear accumulation and target gene expression. Finally, the pharmacological inhibition of PPARα during KD significantly influenced its target gene expression in the gut, but not in the liver. This evidence points toward unique circadian properties of metabolic clocks upon a food stress, even when the same molecular player, such as PPARα, is implicated. Furthermore the liver and intestine clock exhibited different sensitivity to perturbations in the diet macronutrient. Indeed, the hepatic clock was refractory to carbohydrate supplementation under KD, maintaining almost unvaried gene expression. This is in sharp contrast to the intestinal clock that is highly plastic to either sucrose or fructose complementation, as visualized by the changes in gene expression as compared to KD (Figures 6C and 6D). Thus, the sole KD complementation by either sucrose or fructose appears to restore the metabolic clock in the gut to the CC scenario, stressing the specificity in the response of distinct peripheral clocks to food challenges.

An interesting facet of this study relates to the cyclic profile of βOHB upon KD feeding. From a clinical point of view, this notion could be relevant since KD has been broadly used for the treatment of epilepsy (van der Louw et al., 2016). Indeed, circadian control might contribute to the intricate and still poorly explored relationship between seizure control and serum levels of ketone bodies (Gilbert et al., 2000; McNally and Hartman, 2012). Moreover, KD seems to be beneficial as an adjuvant for cancer therapy (Allen et al., 2014; Wright and Simone, 2016), and in obesity, diabetes, and some inherited metabolic disorders (Mobbs et al., 2013; Scholl-Bürgi et al., 2015). Remarkably, βOHB has been demonstrated to be protective in a variety of conditions, such as neurodegenerative diseases (Kashiwaya et al., 2000; Lim et al., 2011), in support of a view in which ketone bodies may have multiple functions in addition to energy source (Puchalska and Crawford, 2017). Our findings support a role of βOHB as an epigenetic regulator in keeping with previous studies (Shimazu et al., 2013; Sleiman et al., 2016). Intriguingly, the rhythmic nature of βOHB in the serum and locally in the gut upon KD is translated into a time-of-the-day-dependent modulation of HDAC activity specifically in the intestine, resulting in differences in the level of histone H3 acetylation and paralleled circadian changes in gene expression. The oscillatory levels of βOHB appear to drive effects on histone acetylation in a tissue-specific manner, being robust in the gut and almost absent in the liver. While the reasons for this intriguing difference are yet to be explored, our data reveal new avenues of future directions to better understand the impact of βOHB, and possibly other metabolites, on the epigenetic landscape and gene expression control of different peripheral clocks.

Finally, our study brings further evidence to the link between chromatin remodeling, diurnal rhythms, and cell energy metabolism. Additional experiments will determine whether KD and the subsequent βOHB oscillation could influence the levels and/or rhythmicity of histone β-hydroxyl-butyrylation, a recently described epigenetic mark involved in metabolic regulation of transcription (Xie et al., 2016).

Our work contributes to the concept that metabolic cues can influence chromatin landscape and gene expression (Katada et al., 2012; Martinez-Pastor et al., 2013) and points to the ability of the clock system to interpret changes in the nutritional regimen in a tissue-specific fashion, leading to distinct rhythmic signatures that designate the physiology and function of the tissue analyzed (Figure 7). It is noteworthy that while the genes and enzymes studied here are expressed in both the ileum and the liver, the clock has the unique ability to recruit them to carry out precise temporal roles tailored for tissue-specific response.

STAR★METHODS

Detailed methods are provided in the online version of this paper and include the following:

- KEY RESOURCES TABLE
- CONTACT FOR REAGENT AND RESOURCE SHARING

SUPPLEMENTAL INFORMATION

Supplemental Information includes seven figures and seven tables and can be found with this article online at http://dx.doi.org/10.1016/j.cmet.2017.08.015.

AUTHOR CONTRIBUTIONS

P.T. and M.M. performed all the experiment. K.L.E.-M. helped in collecting samples and in interpreting the data. Y.L. and P.B. performed the bioinformatic analyses. J.C.N. and E.V. helped in data discussion and project design. P.T., M.M., and P.S.-C. designed the study, prepared the figures, and wrote the manuscript.

ACKNOWLEDGMENTS

We thank all the members of Sassone-Corsi laboratory for constructive comments and Selma Masri for critical discussions. We thank Melanie Oakes, Seung-Ah Chung, and Valentina Ciobanu of the UCI Genomics High-Throughput Facility. We are grateful to Haig Derderian for help and Qin Yang for access to his laboratory's instrumentation. This work was supported by NIH grant DA036408, the Institute National de la Sante et de la Recherche Medicale (INSERM, France) INSERM-44790 and the Novo Nordisk Foundation Challenge Grant NNF-202585 (P.S.-C.), and the Japan Foundation for Pediatric Research 13-003 (M.M.). M.M. was supported by the Sumitomo Life Welfare and Culture Foundation and P.T. was supported by EMBO ALTF 1510-2012 and Human Frontiers Science Program LT 000576/2013.

Received: October 27, 2016
Revised: May 4, 2017
Accepted: August 15, 2017
Published: September 5, 2017

REFERENCES

Agostinelli, F., Ceglia, N., Shahbaba, B., Sassone-Corsi, P., and Baldi, P. (2016). What time is it? Deep learning approaches for circadian rhythms. Bioinformatics *32*, 3051.

Allen, B.G., Bhatia, S.K., Anderson, C.M., Eichenberger-Gilmore, J.M., Sibenaller, Z.A., Mapuskar, K.A., Schoenfeld, J.D., Buatti, J.M., Spitz, D.R., and Fath, M.A. (2014). Ketogenic diets as an adjuvant cancer therapy: history and potential mechanism. Redox Biol. *2*, 963–970.

Asher, G., and Sassone-Corsi, P. (2015). Time for food: the intimate interplay between nutrition, metabolism, and the circadian clock. Cell *161*, 84–92.

Asher, G., Gatfield, D., Stratmann, M., Reinke, H., Dibner, C., Kreppel, F., Mostoslavsky, R., Alt, F.W., and Schibler, U. (2008). SIRT1 regulates circadian clock gene expression through PER2 deacetylation. Cell *134*, 317–328.

Badman, M.K., Pissios, P., Kennedy, A.R., Koukos, G., Flier, J.S., and Maratos-Flier, E. (2007). Hepatic fibroblast growth factor 21 is regulated by PPARalpha and is a key mediator of hepatic lipid metabolism in ketotic states. Cell Metab. *5*, 426–437.

Baldi, P., and Long, A.D. (2001). A Bayesian framework for the analysis of microarray expression data: regularized t -test and statistical inferences of gene changes. Bioinformatics *17*, 509–519.

Bass, J., and Takahashi, J.S. (2010). Circadian integration of metabolism and energetics. Science *330*, 1349–1354.

Bellet, M.M., Deriu, E., Liu, J.Z., Grimaldi, B., Blaschitz, C., Zeller, M., Edwards, R.A., Sahar, S., Dandekar, S., Baldi, P., et al. (2013). Circadian clock regulates the host response to Salmonella. Proc. Natl. Acad. Sci. USA *110*, 9897–9902.

Chavan, R., Feillet, C., Costa, S.S., Delorme, J.E., Okabe, T., Ripperger, J.A., and Albrecht, U. (2016). Liver-derived ketone bodies are necessary for food anticipation. Nat. Commun. *7*, 10580.

Daily, K., Patel, V.R., Rigor, P., Xie, X., and Baldi, P. (2011). MotifMap: integrative genome-wide maps of regulatory motif sites for model species. BMC Bioinformatics *12*, 495.

Debruyne, J.P., Noton, E., Lambert, C.M., Maywood, E.S., Weaver, D.R., and Reppert, S.M. (2006). A clock shock: mouse CLOCK is not required for circadian oscillator function. Neuron *50*, 465–477.

Douris, N., Melman, T., Pecherer, J.M., Pissios, P., Flier, J.S., Cantley, L.C., Locasale, J.W., and Maratos-Flier, E. (2015). Adaptive changes in amino acid metabolism permit normal longevity in mice consuming a low-carbohydrate ketogenic diet. Biochim. Biophys. Acta *1852* (10 Pt A), 2056–2065.

Eckel-Mahan, K., and Sassone-Corsi, P. (2013). Metabolism and the circadian clock converge. Physiol. Rev. *93*, 107–135.

Eckel-Mahan, K.L., Patel, V.R., Mohney, R.P., Vignola, K.S., Baldi, P., and Sassone-Corsi, P. (2012). Coordination of the transcriptome and metabolome by the circadian clock. Proc. Natl. Acad. Sci. USA *109*, 5541–5546.

Eckel-Mahan, K.L., Patel, V.R., de Mateo, S., Orozco-Solis, R., Ceglia, N.J., Sahar, S., Dilag-Penilla, S.A., Dyar, K.A., Baldi, P., and Sassone-Corsi, P. (2013). Reprogramming of the circadian clock by nutritional challenge. Cell *155*, 1464–1478.

Everett, L.J., and Lazar, M.A. (2014). Nuclear receptor Rev-erbα: up, down, and all around. Trends Endocrinol. Metab. *25*, 586–592.

Fukao, T., Lopaschuk, G.D., and Mitchell, G.A. (2004). Pathways and control of ketone body metabolism: on the fringe of lipid biochemistry. Prostaglandins Leukot. Essent. Fatty Acids *70*, 243–251.

Genzer, Y., Dadon, M., Burg, C., Chapnik, N., and Froy, O. (2015). Ketogenic diet delays the phase of circadian rhythms and does not affect AMP-activated protein kinase (AMPK) in mouse liver. Mol. Cell. Endocrinol. *417*, 124–130.

Gilbert, D.L., Pyzik, P.L., and Freeman, J.M. (2000). The ketogenic diet: seizure control correlates better with serum beta-hydroxybutyrate than with urine ketones. J. Child Neurol. *15*, 787–790.

Grygiel-Górniak, B. (2014). Peroxisome proliferator-activated receptors and their ligands: nutritional and clinical implications–a review. Nutr. J. *13*, 17.

Hashim, S.A., and VanItallie, T.B. (2014). Ketone body therapy: from the ketogenic diet to the oral administration of ketone ester. J. Lipid Res. *55*, 1818–1826.

Hatori, M., Vollmers, C., Zarrinpar, A., DiTacchio, L., Bushong, E.A., Gill, S., Leblanc, M., Chaix, A., Joens, M., Fitzpatrick, J.A., et al. (2012). Time-restricted feeding without reducing caloric intake prevents metabolic diseases in mice fed a high-fat diet. Cell Metab. *15*, 848–860.

Hawley, J.A., Hargreaves, M., Joyner, M.J., and Zierath, J.R. (2014). Integrative biology of exercise. Cell *159*, 738–749.

Huang, W., Sherman, B.T., and Lempicki, R.A. (2009). Systematic and integrative analysis of large gene lists using DAVID bioinformatics resources. Nat. Protoc. *4*, 44–57.

Hughes, M.E., Hogenesch, J.B., and Kornacker, K. (2010). JTK_CYCLE: an efficient nonparametric algorithm for detecting rhythmic components in genome-scale data sets. J. Biol. Rhythms *25*, 372–380.

Kashiwaya, Y., Takeshima, T., Mori, N., Nakashima, K., Clarke, K., and Veech, R.L. (2000). D-beta-hydroxybutyrate protects neurons in models of Alzheimer's and Parkinson's disease. Proc. Natl. Acad. Sci. USA *97*, 5440–5444.

Katada, S., Imhof, A., and Sassone-Corsi, P. (2012). Connecting threads: epigenetics and metabolism. Cell *148*, 24–28.

Kayala, M.A., and Baldi, P. (2012). Cyber-T web server: differential analysis of high-throughput data. Nucleic Acids Res. *40*, W553–W559.

Kennedy, A.R., Pissios, P., Otu, H., Roberson, R., Xue, B., Asakura, K., Furukawa, N., Marino, F.E., Liu, F.F., Kahn, B.B., et al. (2007). A high-fat, ketogenic diet induces a unique metabolic state in mice. Am. J. Physiol. Endocrinol. Metab. *292*, E1724–E1739.

Kersten, S., Seydoux, J., Peters, J.M., Gonzalez, F.J., Desvergne, B., and Wahli, W. (1999). Peroxisome proliferator-activated receptor alpha mediates the adaptive response to fasting. J. Clin. Invest. *103*, 1489–1498.

Kohsaka, A., Laposky, A.D., Ramsey, K.M., Estrada, C., Joshu, C., Kobayashi, Y., Turek, F.W., and Bass, J. (2007). High-fat diet disrupts behavioral and molecular circadian rhythms in mice. Cell Metab. *6*, 414–421.

Koike, N., Yoo, S.H., Huang, H.C., Kumar, V., Lee, C., Kim, T.K., and Takahashi, J.S. (2012). Transcriptional architecture and chromatin landscape of the core circadian clock in mammals. Science *338*, 349–354.

Leone, T.C., Weinheimer, C.J., and Kelly, D.P. (1999). A critical role for the peroxisome proliferator-activated receptor alpha (PPARalpha) in the cellular fasting response: the PPARalpha-null mouse as a model of fatty acid oxidation disorders. Proc. Natl. Acad. Sci. USA *96*, 7473–7478.

Leone, V., Gibbons, S.M., Martinez, K., Hutchison, A.L., Huang, E.Y., Cham, C.M., Pierre, J.F., Heneghan, A.F., Nadimpalli, A., Hubert, N., et al. (2015). Effects of diurnal variation of gut microbes and high-fat feeding on host circadian clock function and metabolism. Cell Host Microbe *17*, 681–689.

Lim, S., Chesser, A.S., Grima, J.C., Rappold, P.M., Blum, D., Przedborski, S., and Tieu, K. (2011). D-β-hydroxybutyrate is protective in mouse models of Huntington's disease. PLoS One *6*, e24620.

Martinez-Pastor, B., Cosentino, C., and Mostoslavsky, R. (2013). A tale of metabolites: the cross-talk between chromatin and energy metabolism. Cancer Discov. *3*, 497–501.

Masri, S., Rigor, P., Cervantes, M., Ceglia, N., Sebastian, C., Xiao, C., Roqueta-Rivera, M., Deng, C., Osborne, T.F., Mostoslavsky, R., et al. (2014). Partitioning circadian transcription by SIRT6 leads to segregated control of cellular metabolism. Cell *158*, 659–672.

McNally, M.A., and Hartman, A.L. (2012). Ketone bodies in epilepsy. J. Neurochem. *121*, 28–35.

Mobbs, C.V., Mastaitis, J., Isoda, F., and Poplawski, M. (2013). Treatment of diabetes and diabetic complications with a ketogenic diet. J. Child Neurol. *28*, 1009–1014.

Mohawk, J.A., Green, C.B., and Takahashi, J.S. (2012). Central and peripheral circadian clocks in mammals. Annu. Rev. Neurosci. *35*, 445–462.

Mukherji, A., Kobiita, A., Ye, T., and Chambon, P. (2013). Homeostasis in intestinal epithelium is orchestrated by the circadian clock and microbiota cues transduced by TLRs. Cell *153*, 812–827.

Murakami, M., Tognini, P., Liu, Y., Eckel-Mahan, K.L., Baldi, P., and Sassone-Corsi, P. (2016). Gut microbiota directs PPARγ-driven reprogramming of the liver circadian clock by nutritional challenge. EMBO Rep. *17*, 1292–1303.

Nakahata, Y., Kaluzova, M., Grimaldi, B., Sahar, S., Hirayama, J., Chen, D., Guarente, L.P., and Sassone-Corsi, P. (2008). The NAD+-dependent deacetylase SIRT1 modulates CLOCK-mediated chromatin remodeling and circadian control. Cell *134*, 329–340.

Nakahata, Y., Sahar, S., Astarita, G., Kaluzova, M., and Sassone-Corsi, P. (2009). Circadian control of the NAD+ salvage pathway by CLOCK-SIRT1. Science *324*, 654–657.

Newman, J.C., and Verdin, E. (2014). Ketone bodies as signaling metabolites. Trends Endocrinol. Metab. *25*, 42–52.

Oishi, K., Uchida, D., Ohkura, N., Doi, R., Ishida, N., Kadota, K., and Horie, S. (2009). Ketogenic diet disrupts the circadian clock and increases hypofibrinolytic risk by inducing expression of plasminogen activator inhibitor-1. Arterioscler. Thromb. Vasc. Biol. *29*, 1571–1577.

Okamura, H. (2004). Clock genes in cell clocks: roles, actions, and mysteries. J. Biol. Rhythms *19*, 388–399.

Paoli, A., Rubini, A., Volek, J.S., and Grimaldi, K.A. (2013). Beyond weight loss: a review of the therapeutic uses of very-low-carbohydrate (ketogenic) diets. Eur. J. Clin. Nutr. *67*, 789–796.

Paoli, A., Bosco, G., Camporesi, E.M., and Mangar, D. (2015). Ketosis, ketogenic diet and food intake control: a complex relationship. Front. Psychol. *6*, 27.

Partch, C.L., Green, C.B., and Takahashi, J.S. (2014). Molecular architecture of the mammalian circadian clock. Trends Cell Biol. *24*, 90–99.

Patel, V.R., Eckel-Mahan, K., Sassone-Corsi, P., and Baldi, P. (2012). CircadiOmics: integrating circadian genomics, transcriptomics, proteomics and metabolomics. Nat. Methods *9*, 772–773.

Patel, V.R., Ceglia, N., Zeller, M., Eckel-Mahan, K., Sassone-Corsi, P., and Baldi, P. (2015). The pervasiveness and plasticity of circadian oscillations: the coupled circadian-oscillators framework. Bioinformatics *31*, 3181–3188.

Puchalska, P., and Crawford, P.A. (2017). Multi-dimensional roles of ketone bodies in fuel metabolism, signaling, and therapeutics. Cell Metab. *25*, 262–284.

Rakhshandehroo, M., Knoch, B., Müller, M., and Kersten, S. (2010). Peroxisome proliferator-activated receptor alpha target genes. PPAR Res. *2010*, http://dx.doi.org/10.1155/2010/612089.

Ramsey, K.M., Yoshino, J., Brace, C.S., Abrassart, D., Kobayashi, Y., Marcheva, B., Hong, H.K., Chong, J.L., Buhr, E.D., Lee, C., et al. (2009). Circadian clock feedback cycle through NAMPT-mediated NAD+ biosynthesis. Science *324*, 651–654.

Rardin, M.J., He, W., Nishida, Y., Newman, J.C., Carrico, C., Danielson, S.R., Guo, A., Gut, P., Sahu, A.K., Li, B., et al. (2013). SIRT5 regulates the mitochondrial lysine succinylome and metabolic networks. Cell Metab. *18*, 920–933.

Rey, G., Cesbron, F., Rougemont, J., Reinke, H., Brunner, M., and Naef, F. (2011). Genome-wide and phase-specific DNA-binding rhythms of BMAL1 control circadian output functions in mouse liver. PLoS Biol. *9*, e1000595.

Ripperger, J.A., and Schibler, U. (2006). Rhythmic CLOCK-BMAL1 binding to multiple E-box motifs drives circadian Dbp transcription and chromatin transitions. Nat. Genet. *38*, 369–374.

Schibler, U., and Sassone-Corsi, P. (2002). A web of circadian pacemakers. Cell *111*, 919–922.

Scholl-Bürgi, S., Höller, A., Pichler, K., Michel, M., Haberlandt, E., and Karall, D. (2015). Ketogenic diets in patients with inherited metabolic disorders. J. Inherit. Metab. Dis. *38*, 765–773.

Shimazu, T., Hirschey, M.D., Hua, L., Dittenhafer-Reed, K.E., Schwer, B., Lombard, D.B., Li, Y., Bunkenborg, J., Alt, F.W., Denu, J.M., et al. (2010). SIRT3 deacetylates mitochondrial 3-hydroxy-3-methylglutaryl CoA synthase 2 and regulates ketone body production. Cell Metab. *12*, 654–661.

Shimazu, T., Hirschey, M.D., Newman, J., He, W., Shirakawa, K., Le Moan, N., Grueter, C.A., Lim, H., Saunders, L.R., Stevens, R.D., et al. (2013). Suppression of oxidative stress by β-hydroxybutyrate, an endogenous histone deacetylase inhibitor. Science *339*, 211–214.

Sleiman, S.F., Henry, J., Al-Haddad, R., El Hayek, L., Abou Haidar, E., Stringer, T., Ulja, D., Karuppagounder, S.S., Holson, E.B., Ratan, R.R., et al. (2016). Exercise promotes the expression of brain derived neurotrophic factor (BDNF) through the action of the ketone body β-hydroxybutyrate. Elife *5*, http://dx.doi.org/10.7554/eLife.15092.

Stokkan, K.A., Yamazaki, S., Tei, H., Sakaki, Y., and Menaker, M. (2001). Entrainment of the circadian clock in the liver by feeding. Science *291*, 490–493.

Summa, K.C., Voigt, R.M., Forsyth, C.B., Shaikh, M., Cavanaugh, K., Tang, Y., Vitaterna, M.H., Song, S., Turek, F.W., and Keshavarzian, A. (2013). Disruption of the circadian clock in mice increases intestinal permeability and promotes alcohol-induced hepatic pathology and inflammation. PLoS One *8*, e67102.

Tamanini, F., Chaves, I., Bajek, M.I., and van der Horst, G.T. (2007). Structure function analysis of mammalian cryptochromes. Cold Spring Harb. Symp. Quant. Biol. *72*, 133–139.

Tognini, P., Thaiss, C.A., Elinav, E., and Sassone-Corsi, P. (2017). Circadian coordination of antimicrobial responses. Cell Host Microbe *22*, 185–192.

van der Louw, E., van den Hurk, D., Neal, E., Leiendecker, B., Fitzsimmon, G., Dority, L., Thompson, L., Marchió, M., Dudzińska, M., Dressler, A., et al. (2016). Ketogenic diet guidelines for infants with refractory epilepsy. Eur. J. Paediatr. Neurol. *20*, 798–809.

Veech, R.L. (2014). Ketone ester effects on metabolism and transcription. J. Lipid Res. *55*, 2004–2006.

Vollmers, C., Gill, S., DiTacchio, L., Pulivarthy, S.R., Le, H.D., and Panda, S. (2009). Time of feeding and the intrinsic circadian clock drive rhythms in hepatic gene expression. Proc. Natl. Acad. Sci. USA *106*, 21453–21458.

Wright, C., and Simone, N.L. (2016). Obesity and tumor growth: inflammation, immunity, and the role of a ketogenic diet. Curr. Opin. Clin. Nutr. Metab. Care *19*, 294–299.

Xie, X., Rigor, P., and Baldi, P. (2009). MotifMap: a human genome-wide map of candidate regulatory motif sites. Bioinformatics *25*, 167–174.

Xie, Z., Zhang, D., Chung, D., Tang, Z., Huang, H., Dai, L., Qi, S., Li, J., Colak, G., Chen, Y., et al. (2016). Metabolic regulation of gene expression by histone lysine β-hydroxybutyrylation. Mol. Cell *62*, 194–206.

STAR★METHODS

KEY RESOURCES TABLE

REAGENT or RESOURCE	SOURCE	IDENTIFIER
Antibodies		
Anti-BMAL1 antibody	Abcam	ab93806; RRID: AB_10675117
Anti-PPARα antibody	Santa Cruz Biotechnology	Sc-9000; RRID: AB_2165737
Anti-P84 antibody	GeneTex	GTX70220; RRID: AB_372637
Anti-H3K9/14Ac antibody	Diagenode	C15410200; RRID: AB_2637059
Normal Rabbit IgG	Santa Cruz Biotechnology	SC-2027; RRID: AB_737197
Biological Samples		
Mouse Liver	This paper	See Experimental Model and Subject Details
Mouse Intestine	This paper	See Experimental Model and Subject Details
Mouse Serum	This paper	See Experimental Model and Subject Details
Chemicals, Peptides, and Recombinant Proteins		
GW6471 PPARα inhibitor	Cayman Chemical	11697
Disuccinimidyl Glutarate (DSG)	Thermo Scientific	20593
Trizol Lysis Reagent	Ambion	155696-018
Protein G Sepharose, Fast Flow	Sigma-Aldrich	P3296
Critical Commercial Assays		
β-Hydroxybutyrate LiquiColor Test (Endpoint)	Stanbio	2440-058
BHB Assay Kit	Abcam	ab83390
Free Fatty Acid Quantitation Kit	Sigma-Aldrich	MAK044
Cholesterol Quantitation Kit	Sigma-Aldrich	MAK043
HDAC Assay Kit	Active Motif	56200
Deposited Data		
Liver and IECs circadian microarray dataset	This paper	GEO: GSE87425
Experimental Models: Organisms/Strains		
Male C57BL/6J mice	Jackson Laboratory	000664
Male *Clock*-deficient mice	Laboratory of Dr. S. Reppert (Worcester, MA)	Debruyne et al., 2006
Oligonucleotides		
Primers for RT-PCR, see Table S7	This paper	N/A
Software and Algorithms		
JTK_CYCLE	Hughes et al., 2010	N/A
BIO_CYCLE	Agostinelli et al., 2016	N/A
DAVID v6.7	N/A	N/A
GeneChip Scanner 3000 7G	N/A	N/A
Command Console Software v. 3.2.3	N/A	N/A
Other		
Control Chow Diet (CC)	Envigo, Teklad Custom diet	TD.150345
Ketogenic Diet (KD)	Envigo, Teklad Custom diet	TD.160153
1,3-Butanediol diet (BD)	Envigo, Teklad Custom diet	TD. 160257

CONTACT FOR REAGENT AND RESOURCE SHARING

Further information and requests for resources and reagents should be directed to and will be fulfilled by the Lead Contact, Paolo Sassone-Corsi (psc@uci.edu).

EXPERIMENTAL MODEL AND SUBJECT DETAILS

Animals and Feeding

Eight week-old male C57BL/6J mice (JAX, 00064), maintained at 24°C on a 12 hr light/ 12 hr dark cycle, were fed ad libitum to a ketogenic diet (KD, Envigo, Teklad Custom diet TD.160153, 90.5% kcal from fat, 9.5% kcal from protein), to a control chow (CC, Envigo Teklad Custom diet TD.150345, 12.6% kcal from fat, 9.8% kcal from protein, 77.7% from carbohydrate) or to 1,3-Butanediol diet (10% 1,3-butanediol) (BD, Envigo, Teklad Custom diet TD. 160257) for 4 weeks.

At the end of the 4 weeks 5-7 mice per time-point, per group were sacrificed via CO_2 and cervical dislocation every four hours along the diurnal cycle (from ZT0 to ZT24). *Clock*-deficient animals were a gift from S. Reppert (Worcester, MA). Study animals were backcrossed to the C57BL/6 background for four generations (Debruyne et al., 2006). Eight week-old male *Clock*-deficient mice and their WT littermates were maintained in the same condition described for C57BL/6J. 4-5 *Clock*-deficient animals or WT littermates per time-point were sacrificed via CO_2 and cervical dislocation at ZT12 (light off, starting of the active phase). Liver and intestine were harvested from both C57BL/6J mice and *Clock*-deficient mice and immediately frozen in liquid nitrogen. A portion of the ileum was processed for intestinal epithelial cells isolation as reported below.

A second cohort of animals was sacrificed at ZT0-8-12-20 (n = 5 per time-point) during an independent experiment. Animal care and use was in accordance with guidelines of the institutional Animal Care and Use Committee at the University of California at Irvine.

METHOD DETAILS

Mouse Diets

All diets are matched on a per-calorie basis for micronutrient content, fiber, and preservatives.

The composition of the three experimental diets (CC = control chow, KD = Ketogenic diet, BD = 1,3-Butanediol diet) is as follows (g/Kg):

	CC TD.150345	KD TD.160153	BD TD.160257
Casein	100	180	106.44
DL-methionine	1.6	2.88	1.7
Corn starch	512.46	0	436.973
Sucrose	100	0	85
Maltodextrin	155	0	130.5
Crisco	25	440	0
Cocoa butter	0	150	0
Corn oil	25	85	26.6
Cellulose	35	59.19	37.17
1,3 Butanediol	0	0	100
Calories per gram	3.6	6.7	3.9

Vitamin supplements included AIN-93-VX vitamin mix (Envigo 110068), thiamin, phylloquinone, choline bitartate, mineral mix (Envigo 98057), calcium phosphate, and calcium carbonate. Crisco is a proprietary blend of partially hydrogenated vegetable oil, with minimal trans-fat content. Fatty acids in KD are, by weight, approximately 24% saturated, 39% monounsaturated, and 37% polyunsaturated.

GW6471 Treatment

Eight week-old male C57BL/6J mice (JAX, 00064), maintained at 24°C on a 12 hr light/ 12 hr dark cycle, were fed ad libitum to a ketogenic diet (KD, Envigo diet TD. 160153, 90.5% kcal from fat, 9.5% kcal from protein) or to a control chow (CC, Envigo diet TD.150345, 12.6% kcal from fat, 9.8% kcal from protein, 77.7% from carbohydrate) for 4 weeks. Twice per week the animals were intraperitoneally injected once a day (ZT11) with the specific PPARα inhibitor GW6471 (Cayman chemical, Cat. N. 11697), at a dose of 10mg per Kg of body weight. GW6471 was dissolved in DMSO at a concentration of 10mg/ml and diluted in PBS before the injection. At the end of the 4 weeks 3-4 mice per time-point, per group were sacrificed via CO2 and cervical dislocation at ZT8 and at ZT20. Animal care and use was in accordance with guidelines of the institutional Animal Care and Use Committee at the University of California at Irvine.

Fructose and Sucrose Treatment

Eight week-old male C57BL/6J mice, maintained on a 12 hr light/ 12 hr dark cycle, were fed ad libitum to KD or CC for four weeks. The last week of feeding regimen, Fructose (4g/Kg) dissolved in PBS was administered to the mice through oral gavage (Volume = 200ul), once a day for seven days.

For sucrose experiments, mice were supplemented with 30% sucrose in drinking water ad libitum during the four weeks of dietary regimen. At the end of the 4th week animals were sacrificed via CO2 and cervical dislocation at ZT0 (light on) and ZT12 (light off). Liver and intestine were harvested and immediately frozen in liquid nitrogen.

Indirect Calorimetry

Calorimetry was performed as described in Eckel-Mahan et al. (2012), using negative-flow CLAMS hardware system cages (Columbus Instruments, Columbus, Ohio). Briefly, animals were housed at a temperature of 24°C and subjected to individual indirect calorimetry measurements for a period of 5 consecutive days under a 12 hr light/ 12 hr dark cycle. The first 48 hr of the experiment served to allow acclimation of the mouse to the metabolic cage, and were not included in the analysis. Food and water were available ad libitum during the whole experiment. VO2, VCO2, and food intake were measured every 10 min. RER (VCO2/VO2) was calculated with Oxymax software (Columbus Instruments).

Intestinal Epithelial Cells (IECs) Isolation

IECs was isolated as previously described (Mukherji et al., 2013) with slight modifications. Specifically, 12 cm of ileum (0-12 cm upstream of cecum) was taken, opened longitudinally and washed vigorously in Hanks Balanced Salt Solution (HBSS). The samples were put in 10 mM EDTA in HBSS with 5% fetal bovine serum and shaken at 200 rpm for 20 min at 37°C. The supernatant containing IECs was centrifuged (720 g, 5 min, 4°C) and the pellet was washed in PBS. Following centrifugation (720 g, 5 min, 4°C), the pellet was frozen at −80°C for future analysis.

RNA Extraction

Liver samples were homogenized in Trizol Lysis Reagent (Ambion Cat. N. 155696-018). Chloroform was added and the samples were shaken for 15 s. The samples were left at RT for 3 min and then centrifuged (12000 g, 15 min, 4°C). The aqueous solution, containing RNA, was collected in a fresh tube and the RNA was precipitated by the addition of isopropanol. Samples were mixed, left at RT for 10 min and then centrifuged (12000 g, 10 min, 4°C). Supernatant was discarded and the RNA pellet was washed in 75% ethanol by centrifugation (7500 g, 5 min, 4°C). Supernatant was discarded and the pellet was re-suspended in DEPC-treated water. To increase RNA purity, RNA was purified using the RNeasy mini kit (Qiagen Cat. N. 74106). Total RNA concentrations were determined by Nanodrop Spectrophotometer (Thermo Scientific). RNA quality was analyzed via agarose gel electrophoresis (1% agarose). Total RNA was reverse transcribed using Iscript reverse transcription Super mix (Biorad Cat. N. 1708840).

Gene expression was analyzed by Real time PCR (Biorad CFX96 Real-Time System) using SsoAdvanced Universal SYBR Green Supermix (Biorad Cat. N. 172-5270).

Microarray Analysis

All starting total RNA samples were quality assessed prior target preparation/processing steps by running out a small amount of each sample (typically 25-250 ng/well) onto a RNA 6000 Nano LabChip that was evaluated on an Agilent Bioanalyzer 2100 (Agilent Technologies, Palo Alto, CA). Microarray analyses were performed at the Genomics High-Throughput Facility, University of California Irvine.

Gene Ontology Analysis

Gene ontology analysis was performed using Database for Annotation, Visualization and Integrated Discovery (DAVID) v6.7, using genomic background; and Kyoto Encyclopedia of Genes and Genomes (KEGG) pathway was chosen for gene clustering.

Protein Extraction and Western Blot

For whole cell extracts, liver samples were homogenized in modified RIPA buffer (50 mM Tris pH8, 150mM NaCl, 5mm EDTA, 15mM MgCl2, 1% NP40) plus protease inhibitors and centrifuge for 15 min at 14000 g 4oC. The supernatant was recovered and the protein concentration was determined by Bradford assay (Biorad Cat. N. 500-0006).

For liver nuclear fraction, approximately 250 mg of liver was homogenized in 4 mL buffer A (10 mM HEPES, pH 7.8, 25 mM KCl, 0.5 mM spermidine, 1 mM EGTA, 1 mM EDTA, 0.32 M sucrose, 0.3% triton) with protease inhibitors. Samples were centrifuged (1,000 g, 10 min, 4°C) and the pellets were resuspended in 4 mL buffer A. Following centrifugation (1,000 g, 10 min, 4°C), 4 mL low salt buffer (10 mM HEPES, pH 7.8, 25 mM KCl, 0.5 mM spermidine, 1 mM EGTA, 1 mM EDTA, and 20% glycerol) was added to the pellets and then centrifuged again (1,000 g, 10 min, 4°C). The pellets were resuspended in 1 mL low salt buffer, centrifuged, and resuspended in 1x volume low salt buffer and 2x high salt buffer (10 mM HEPES, pH 7.8, 25 mM KCl, 0.5 mM spermidine, 1 mM EGTA, 1 mM EDTA, 20% glycerol, and 0.5 M KCl). Suspensions were nutated for 1 hr at 4°C and then centrifuged (12,000 g, 20 min, 4°C). The resulting supernatant was used as the nuclear fraction. For nuclear fraction of IECs, buffer B (10 mM HEPES-KOH, pH 7.9, 1.5 mM MgCl2, 10 mM KCl) was added to wash the frozen aliquots of IECs and centrifuged (1,000 g, 5min, 4°C). 0.2% NP40 in buffer B was added to the pellets and left on ice for 10min before centrifugation (10,000 g, 5min, 4°C). The pellets were washed with buffer B and centrifuged again (10,000 g, 5min, 4°C). The pellets were re-suspended in modified RIPA (500 mM Tris-HCl, pH 7.4, 1% NP-40, 0.25% deoxycholic acid-Na, 150 mM NaCl, 1mM EDTA), sonicated and centrifuged (12,000 g, 20min, 4°C). The supernatant was used as the nuclear fraction.

8% SDS-PAGE was performed to check BMAL1 and PPARα expression. The samples were blotted onto nitrocellulose membranes (Biorad) and blocked in 5% non-fat dry milk in Tris-buffered saline (TBS) for 2 hr at room temperature RT. The nitrocellulose membrane was incubated at 4°C overnight with the following antibodies: anti-BMAL1 (Abcam ab93806) 1:2000, anti-PPARα (Santa Cruz Biotechnology Sc 9000) 1:1000 and anti-P84 1:3000 (GeneTex GTX70220). Blots were then washed 3 times in TTBS for thirty minutes, incubated in HRP conjugated anti-mouse or anti-rabbit diluted (1:8000) in 2.5% milk in TTBS for one hour at RT. The membranes were than rinsed three times in TTBS and incubated in enhanced chemiluminescent substrate (Millipore Cat. N. WBKLS0500) and exposed to film. The films were scanned and densitometry was analyzed through ImageJ software.

Chromatin Immunoprecipitation (ChIP)

Minced frozen liver or ileum tissue was double crosslinked with DSG for 40 min and 1% formaldehyde for 10 min followed by Glycine (0.125M final concentration) at room temperature for 10 min. After homogenizing tissue pellet in PBS, 1 mL of lysis buffer was added. Samples were sonicated by Bioruptor (20 cycles, every cycle: 30 s ON / 30 s OFF, power high) to generate 200-500 base pairs fragments and centrifuged at 14000 g at 4°C. Supernatants were diluted in dilution buffer (1.1% Triton X-100, 1.2 mM EDTA, 16.7 mM Tris-HCl, 167 mM NaCl), precleared with Protein-G beads, blocked with salmon sperm DNA and BSA for 2 hr. Precleared supernatant was incubated with the following primary antibodies: 2 μg BMAL1 (Abcam Cat. N. ab93806) or 1 μg H3K9/14ac (Diagenode Cat. N. C15410200) overnight at 4°C. To monitor the specificity of ChIP assays, samples were also immunoprecipitated with a specific-antibody isotype matched control immunoglobulin (IgG). Protein-G beads Sepharose, Fast Flow (Sigma-Aldrich Cat. N. P3296) were added to the supernatant and incubated for 2 hr at 4°C and centrifuged. Beads were recovered, washed in low salt buffer, high salt buffer, LiCl buffer, followed by washing in TE for three times. Elution buffer (300 mM NaCl, 0.5% SDS, 10 mM Tris-HCl, 5mM EDTA) was added to the washed beads, treated with RNase at 37°C for 2 hr and Proteinase K at 65°C overnight. Equal amount of Phenol-Chloroform-Isoamyl alcohol was added to the samples and the aqueous phase was recovered. DNA was precipitated by adding 100% Ethanol, NaOAc and glycogen and kept at −20°C overnight. Samples were centrifuged at 14000 g for 30 min at 4°C and washed with 70% ethanol followed by centrifugation at 14000 g for 30 min at 4°C. Quantitative PCRs were performed using SsoAdvanced Universal SYBR Green Supermix (Biorad), according to the manufacturer's protocol.

qPCR Primers

The primers for gene expression and ChIP were designed by Primer 3 software (v. 0.4.0) or obtained from previous publications: Dbp E-box ChIP primers are based on Ripperger and Schibler (2006), and Nampt E-box chip primers are based on Nakahata et al. (2009). All the primer sequences are reported in Table S7.

β-Hydroxyl-Butyrate Quantitation

Fresh blood was centrifuged at 1500 g for 15 min and serum isolated. β-Hydroxyl-butyrate level were quantified using β-Hydroxybutyrate LiquiColor Test (Endpoint) (StanBio Cat. N. 2440-058) according to the manufacturer's instructions. For β-Hydroxybutyrate levels in intestine and liver, we used Abcam BHB Assay kit (Cat. N. ab83390). The samples were prepared and deproteinated with PCA according to the manufacturer's instruction.

Fatty Acid and Cholesterol Quantitation

10-15 mg of liver or intestinal tissue were used to check free fatty acid and total cholesterol levels. Free fatty acid were quantified using the ''Free fatty acid quantitation kit'' (Sigma-Aldrich Cat. N. MAK044) according to manufacturer's instructions. Total cholesterol was quantified using the ''Cholesterol quantitation kit'' (Sigma-Aldrich Cat. N. MAK043) according to manufacturer's instructions.

HDAC Activity Assay

15 μg of intestinal or liver nuclear extract was tested using HDAC assay kit (Active Motif Cat. N. 56200) according to manufacturer's instructions.

QUANTIFICATION AND STATISTICAL ANALYSIS

Microarray Data Analysis and Statistics

3 animals per time-point, per group were analyzed. Arrays were scanned using GeneChip Scanner 3000 7G and Command Console Software v. 3.2.3 to produce .CEL intensity files. The intensity files were then analyzed in Affymetrix Expression Console software v1.1.1 using the PLIER algorithm to generate probe level summarization files (.CHP), where signal levels were normalized between KD and CC conditions within the same tissue. Expression levels time series were then used to determine circadian behaviors of transcripts using JTK-CYCLE (Hughes et al., 2010) and the results were corroborated using BIO_CYCLE (Agostinelli et al., 2016), an improved circadian rhythm analysis software. Circadian behaviors include whether or not a transcript is circadian as well as its phase and amplitude. Both methods produced similar results and importantly, key transcripts such as the core clock genes and PPARα targets showed the same behavior. In the rest of the analysis, we report the results obtained with JTK-CYCLE. For JTK-CYCLE, a gene was considered circadian, if at least one of its transcripts passed a p value cutoff of 0.01. Data visualization was done in Python using 'matplotlib' and R using 'gplots'. The Database for Annotation, Visualization and Integrated Discovery (DAVID) pathway

analysis tool was used to identify GO terms related to biological process and potentially enriched pathways (Huang et al., 2009). Pathways were ranked by the number of circadian genes they contained with a JTK-CYCLE p value < 0.01, and results were compared to the genomic background for enrichment. For the background, we selected all the possible genes in the whole genome that can be detected by the specific microarray (extracted from the microarray annotation). The total number of background genes is around 25,000. The lists of PPARα and BMAL1 target genes used in focused analysis were generated using a combination of literature evidence (Rakhshandehroo et al., 2010), MotifMap (Daily et al., 2011; Xie et al., 2009) and publically available ChIP Seq datasets from GEO (GEO: GSE35262 and GSE39977). Differential analysis of transcript expression levels between KD and CC at certain ZTs was done using CyberT (Baldi and Long, 2001; Kayala and Baldi, 2012), a differential analysis program using a Bayesian-regularized t test. Variance Stabilizing Normalization was used process the data for input to CyberT using the R package 'vsn'. Further statistical analysis including multiple hypothesis testing corrections was done in R using 'fdrtool'.

Analysis was done using pipelines implemented for the Circadiomics (Patel et al., 2012, 2015) database and web portal (http://circadiomics.ics.uci.edu/) where all the transcriptomic data associated with this work is publicly available.

Phase lag analysis was performed based on the "LAG" (predicted phase) obtained by JTK-CYCLE for every single gene (See also Tables S3 and S4). The genes with the same "LAG" were grouped together and the data reported in the radar plot as percentage. Anderson-Darling tests were performed using the R package 'kSamples' to determine whether or not the phase distributions of KD and CC circadian transcripts were statistically different ($p < 0.0001$). Student's t tests were conducted to determine if changes, in terms of JTK amplitudes or specific expression at ZT8, were significant between KD and CC conditions for circadian transcripts.

Transcription Factor Enrichment Analysis

Transcription factors were analyzed in terms of enrichment for binding sites in the promoter regions (−10000∼+2000 bps of TSS) of rhythmic genes in each circadian group, where binding sites were extracted from high quality MotifMap results for the mouse genome build mm9 (BBLS > 1, FDR < 0.25). A Fisher's exact test was performed between the circadian genes and the whole genome to establish enrichment (odds > 1, $p < 0.05$). TFs with motifs that are too short or degenerate (more than 50000 binding sites under the filtering criteria) were removed, as they tend to be unreliable.

Enrichment results for different conditions across circadian groups were then compared in a meta-analysis to identify tissue-specific TFs. As an example, a PPARα related motif was found to be uniquely enriched in IECs under ketogenic diet, when compared to both IECs under normal chow diet or liver under ketogenic diet, which suggests that it may explain the tissue-specific response to ketogenic diet treatment. In contrast, Clock:Bmal motif was found to be enriched in virtually all circadian groups except for ketogenic IECs when compared to ketogenic liver, which suggests that there is a stronger tissue-specific effect of Clock:Bmal controlled genes in ketogenic liver when compared to IECs, despite the fact that Clock:Bmal is virtually ubiquitously enriched as a core circadian TF. Full details of the analysis are provided as Table S6 (sheet 4).

Other Statistical Analysis

Data are expressed as mean ± SEM. The significance of differences was analyzed by Student's t test or two-way ANOVA and post hoc analysis for multiple group comparison. The test was considered significant with a P value < 0.05.

DATA AND SOFTWARE AVAILABILITY

The GEO accession number for the microarray dataset reported in this paper is GEO: GSE87425. All the transcriptomic data associated with this work is publicly available on the resource http://circadiomics.ics.uci.edu/.

Cell Metabolism, Volume *26*

Supplemental Information

Distinct Circadian Signatures in Liver and Gut Clocks Revealed by Ketogenic Diet

Paola Tognini, Mari Murakami, Yu Liu, Kristin L. Eckel-Mahan, John C. Newman, Eric Verdin, Pierre Baldi, and Paolo Sassone-Corsi

Suppl. Fig. 1

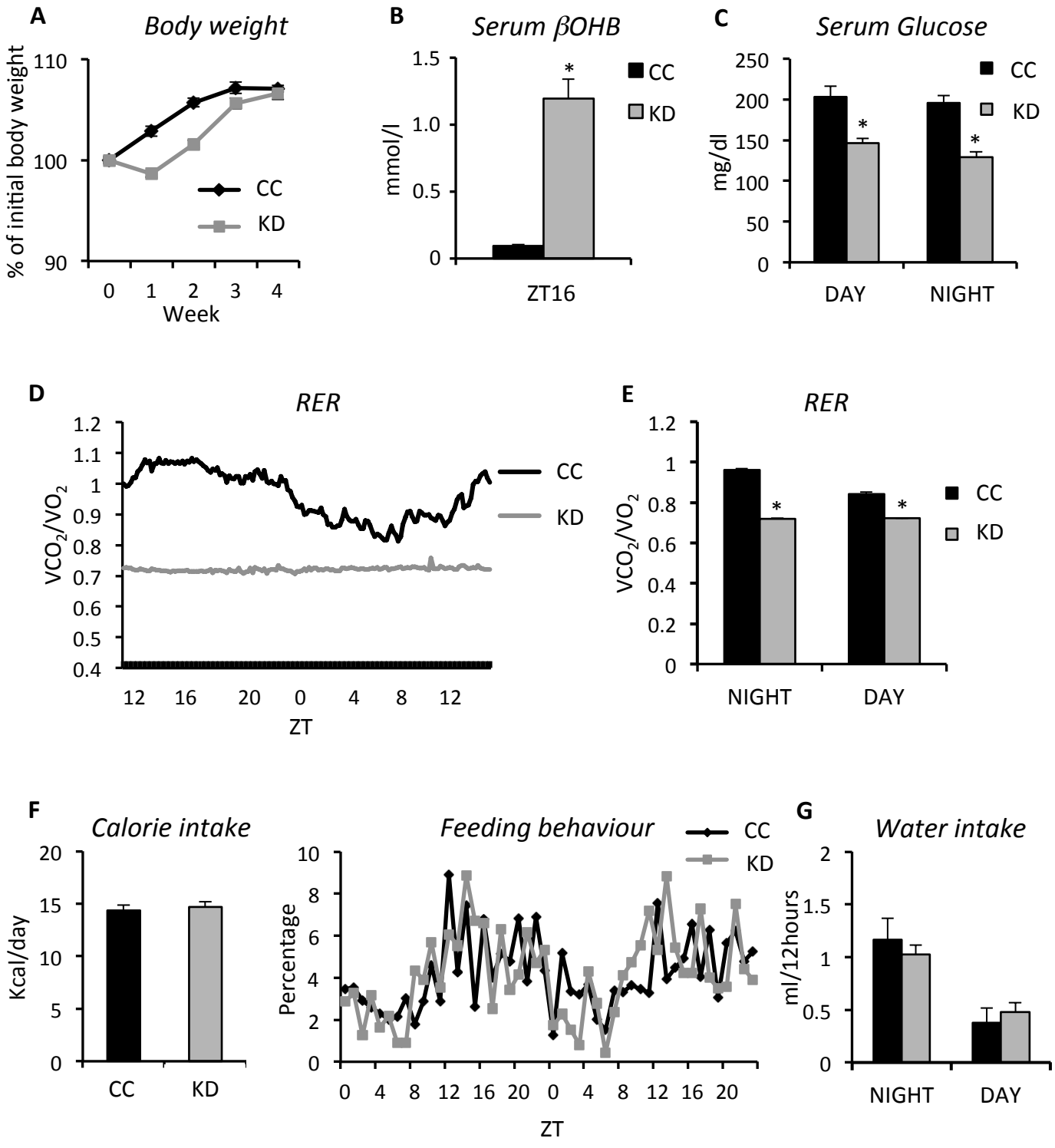
A
Body weight
% of initial body weight
110
100
90
0 1 2 3 4
Week
CC
KD
B
Serum βOHB
mmol/l
1.5
1.0
0.5
0
*
ZT16
CC
KD
C
Serum Glucose
mg/dl
250
200
150
100
50
0
*
*
DAY
NIGHT
CC
KD
D
RER
VCO2/VO2
1.2
1.1
1
0.9
0.8
0.7
0.6
0.5
0.4
12 16 20 0 4 8 12
ZT
CC
KD
E
RER
VCO2/VO2
1.2
1
0.8
0.6
0.4
0.2
0
*
*
NIGHT
DAY
CC
KD
F
Calorie intake
Kcal/day
20
15
10
5
0
CC
KD
Feeding behaviour
Percentage
10
8
6
4
2
0
0 4 8 12 16 20 0 4 8 12 16 20
ZT
CC
KD
G
Water intake
ml/12hours
2
1.5
1
0.5
0
NIGHT
DAY

Suppl. Fig. 2

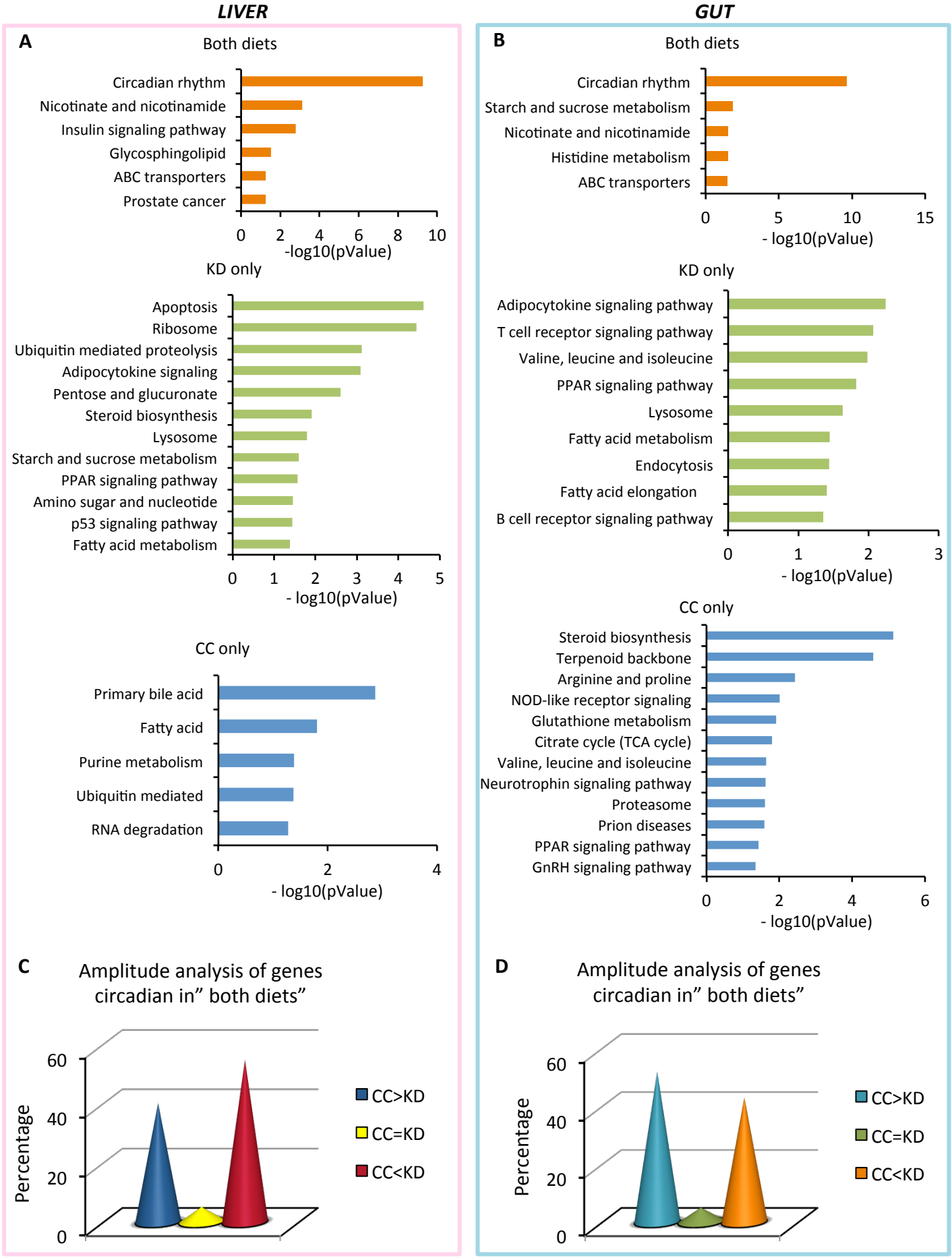
LIVER
GUT
A
Both diets
Circadian rhythm
Nicotinate and nicotinamide
Insulin signaling pathway
Glycosphingolipid
ABC transporters
Prostate cancer
0 2 4 6 8 10
-log10(pValue)
KD only
Apoptosis
Ribosome
Ubiquitin mediated proteolysis
Adipocytokine signaling
Pentose and glucuronate
Steroid biosynthesis
Lysosome
Starch and sucrose metabolism
PPAR signaling pathway
Amino sugar and nucleotide
p53 signaling pathway
Fatty acid metabolism
0 1 2 3 4 5
- log10(pValue)
CC only
Primary bile acid
Fatty acid
Purine metabolism
Ubiquitin mediated
RNA degradation
0 2 4
- log10(pValue)
B
Both diets
Circadian rhythm
Starch and sucrose metabolism
Nicotinate and nicotinamide
Histidine metabolism
ABC transporters
0 5 10 15
- log10(pValue)
KD only
Adipocytokine signaling pathway
T cell receptor signaling pathway
Valine, leucine and isoleucine
PPAR signaling pathway
Lysosome
Fatty acid metabolism
Endocytosis
Fatty acid elongation
B cell receptor signaling pathway
0 1 2 3
- log10(pValue)
CC only
Steroid biosynthesis
Terpenoid backbone
Arginine and proline
NOD-like receptor signaling
Glutathione metabolism
Citrate cycle (TCA cycle)
Valine, leucine and isoleucine
Neurotrophin signaling pathway
Proteasome
Prion diseases
PPAR signaling pathway
GnRH signaling pathway
0 2 4 6
- log10(pValue)
C
Amplitude analysis of genes circadian in" both diets"
Percentage
0 20 40 60
CC>KD
CC=KD
CC<KD
D
Amplitude analysis of genes circadian in" both diets"
Percentage
0 20 40 60
CC>KD
CC=KD
CC<KD

Suppl. Fig. 3

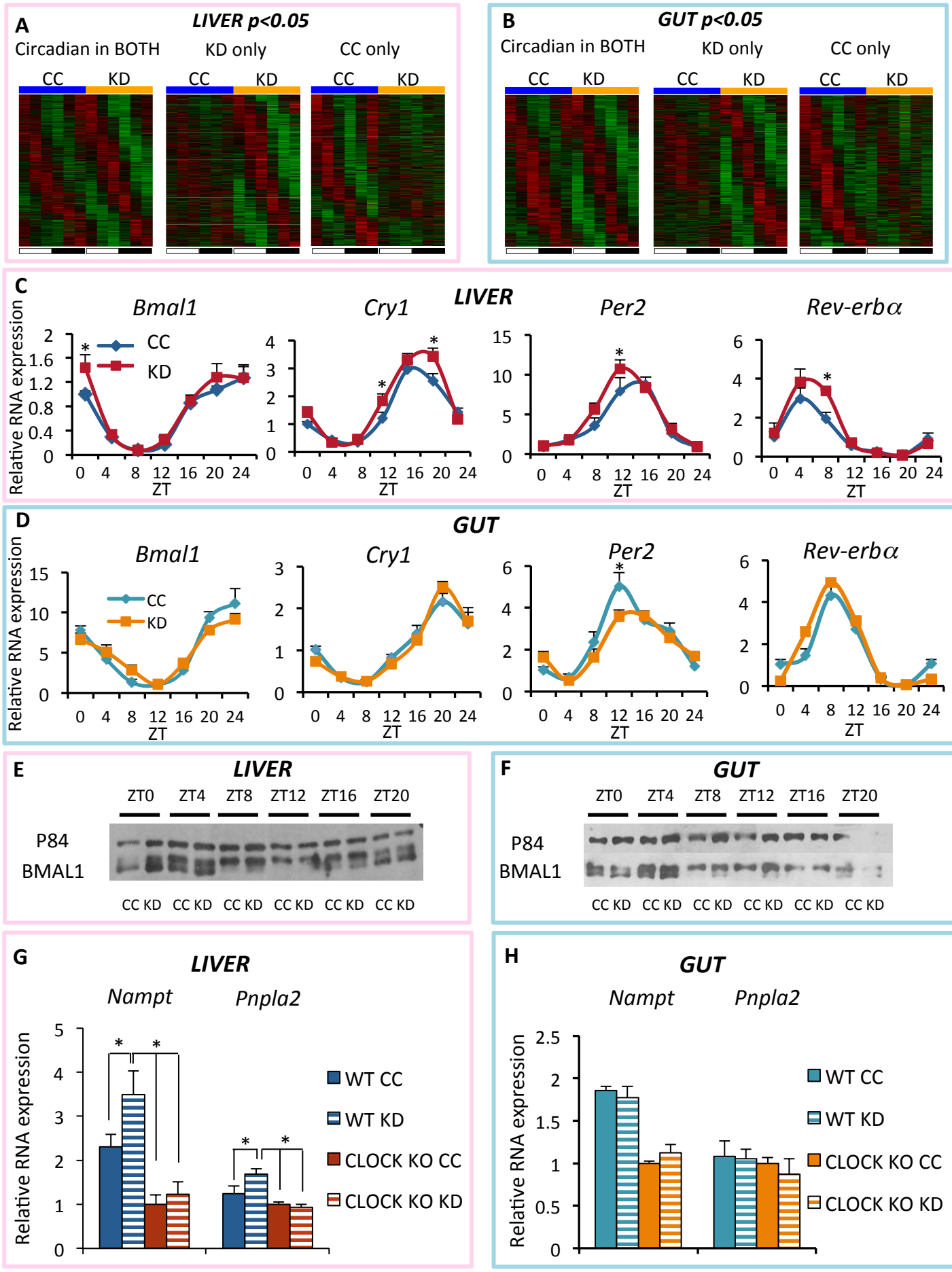
A
LIVER p<0.05
Circadian in BOTH
KD only
CC only
CC
KD
B
GUT p<0.05
C
LIVER
Bmal1
Cry1
Per2
Rev-erbα
Relative RNA expression
ZT
D
GUT
E
LIVER
ZT0 ZT4 ZT8 ZT12 ZT16 ZT20
P84
BMAL1
CC KD
F
GUT
G
LIVER
Nampt
Pnpla2
WT CC
WT KD
CLOCK KO CC
CLOCK KO KD
H
GUT

Suppl. Fig. 4

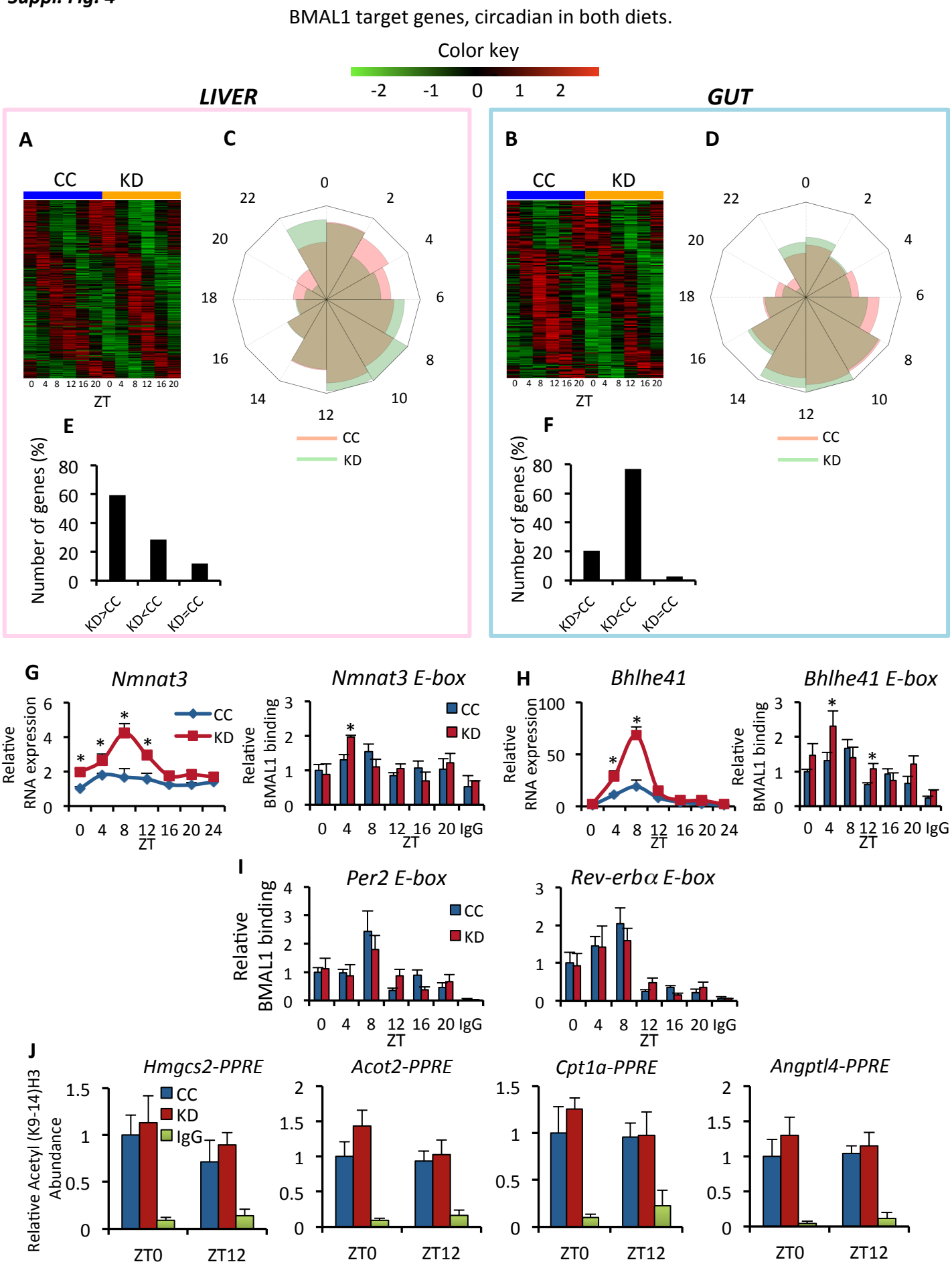
BMAL1 target genes, circadian in both diets.
Color key
-2 -1 0 1 2
LIVER
GUT
A
B
C
D
CC
KD
ZT
E
F
Number of genes (%)
KD>CC
KD<CC
KD=CC
G
Nmnat3
Nmnat3 E-box
H
Bhlhe41
Bhlhe41 E-box
Relative RNA expression
Relative BMAL1 binding
IgG
I
Per2 E-box
Rev-erbα E-box
J
Hmgcs2-PPRE
Acot2-PPRE
Cpt1a-PPRE
Angptl4-PPRE
Relative Acetyl (K9-14)H3 Abundance
ZT0
ZT12

Suppl. Fig. 5 **A** **Pparα target genes organized in specific biological pathways**

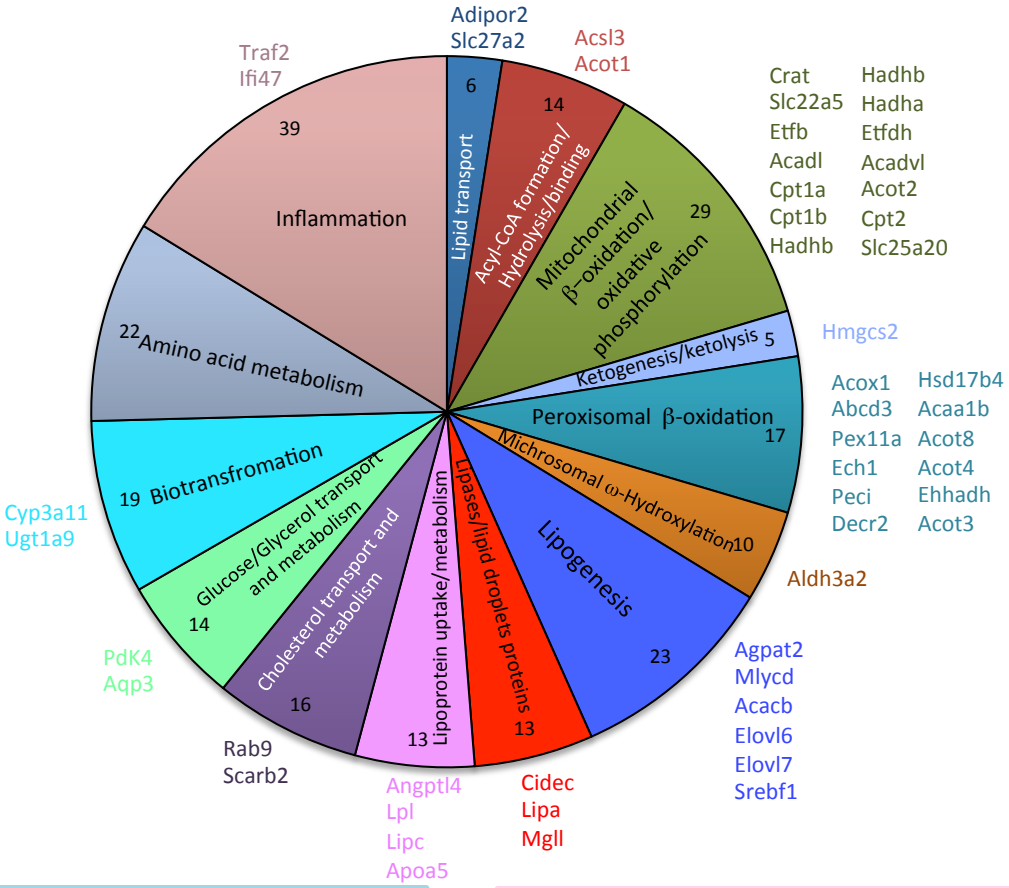

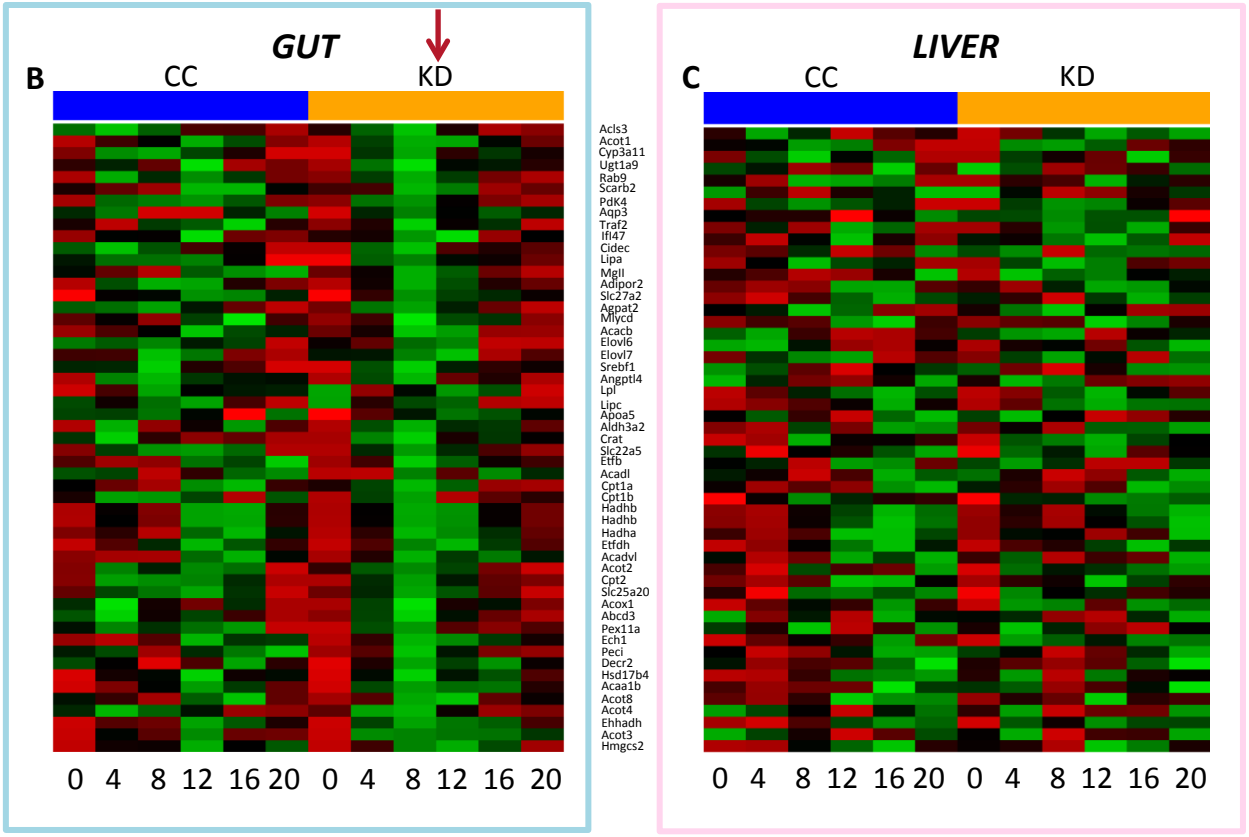

Suppl. Fig. 6

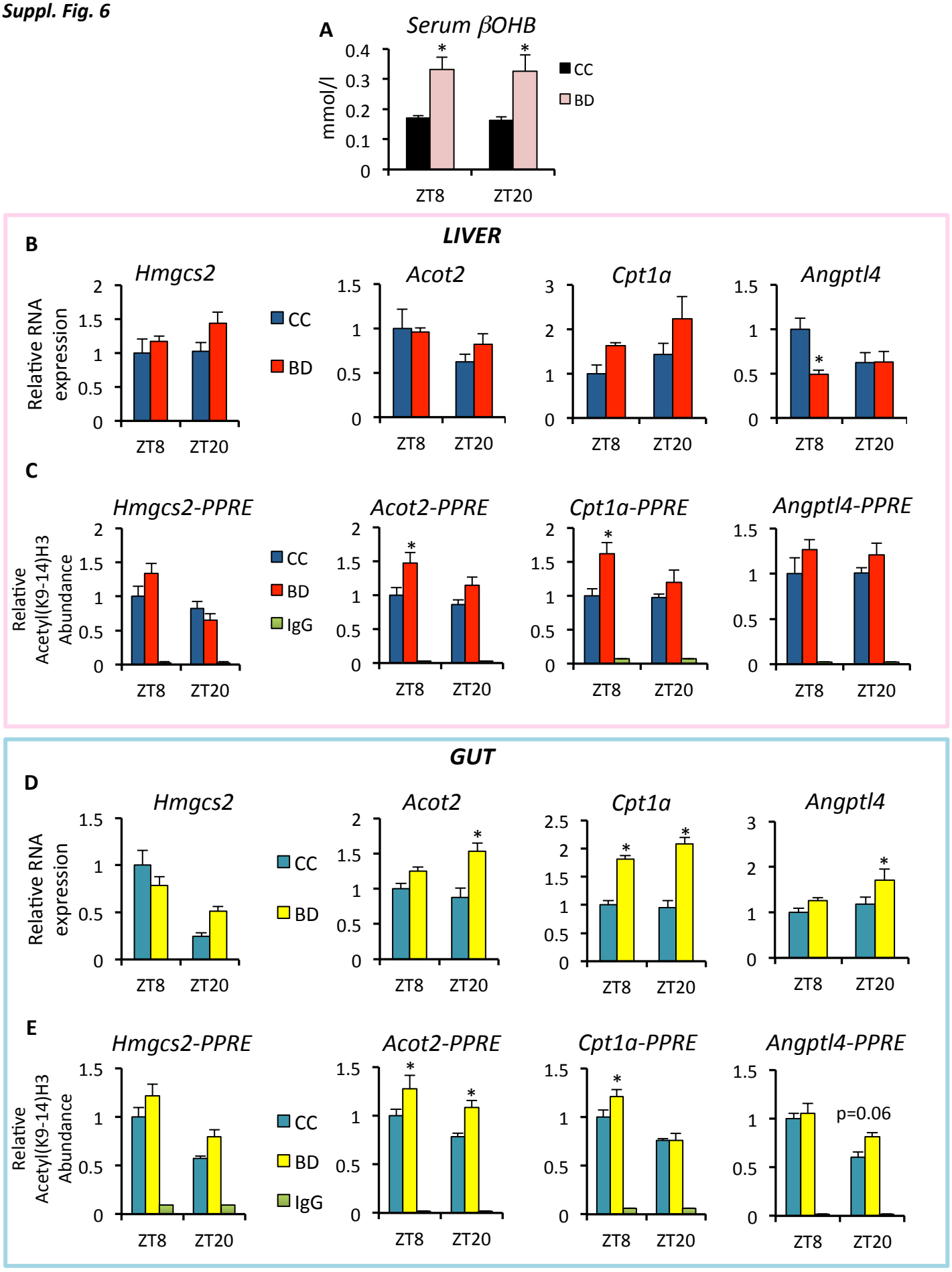
A
Serum βOHB
mmol/l
0.4
0.3
0.2
0.1
0
*
*
CC
BD
ZT8
ZT20
LIVER
B
Hmgcs2
Acot2
Cpt1a
Angptl4
Relative RNA expression
CC
BD
C
Hmgcs2-PPRE
Acot2-PPRE
Cpt1a-PPRE
Angptl4-PPRE
Relative Acetyl(K9-14)H3 Abundance
IgG
GUT
D
E
p=0.06

Suppl. Fig. 7

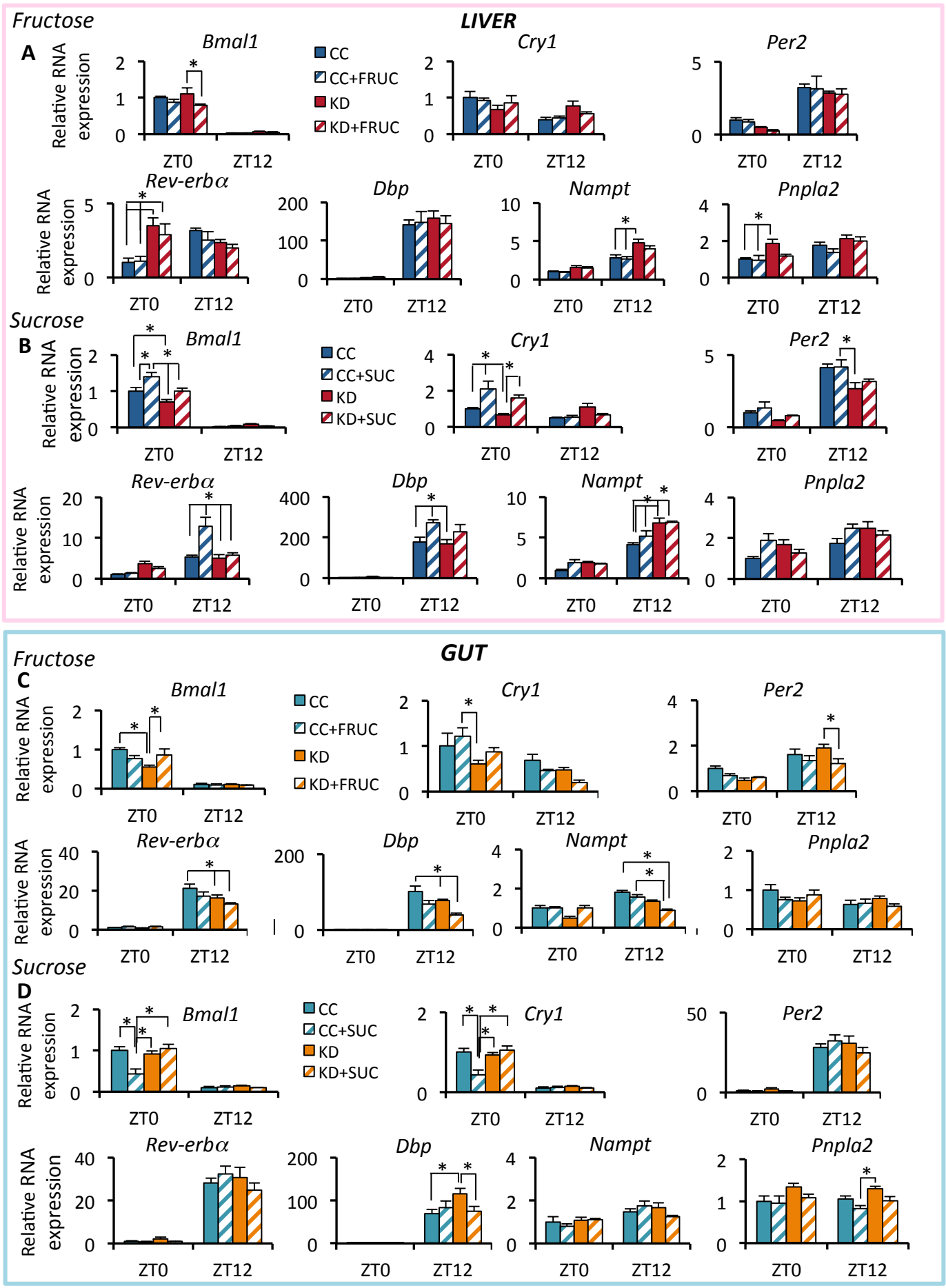
Fructose
LIVER
A
Bmal1
Cry1
Per2
Rev-erbα
Dbp
Nampt
Pnpla2
Relative RNA expression
CC
CC+FRUC
KD
KD+FRUC
ZT0
ZT12
Sucrose
B
CC+SUC
KD+SUC
GUT
C
D

SUPPLEMENTAL FIGURE LEGEND

Figure S1. Metabolic phenotype of KD fed mice. Related to STAR methods section: "Indirect Calorimetry".

(A) Percentage of body weight (n=35 animals per group).
(B) Serum βOHB concentration (n=5 animals per group; Student t-test, *p<0.05).
(C) Serum glucose concentration (n=15 animals per group, per time point; Student t-test, *p<0.05).
(D) Respiratory exchange ratio (RER) of CC and KD mice across a 24h period (n=10 mice per group; two-way ANOVA: time p<0.0001, diet p<0.001, interaction p<0.001).
(E) Average of RER values during night and day-time (n=10 mice per group; Student t-test, *p<0.05).
(F) Calorie intake in CC and KD fed mice and feeding pattern along two daily cycles (n=10 mice per group; Student t-test, no significant difference).
(G) Water intake in CC and KD fed mice (n=10 mice per group; Student t-test, no significant difference).
Error bars represent SEM.

Figure S2. Kyoto Encyclopedia of Genes and Genomes (KEGG) pathways analysis. Related to Figure 1.

(A) Gene ontology (GO) analysis of genes circadian in "both diets", "KD only" and "CC only" in the liver. The negative log (base 10) of the p value [-log10(pvalue)] was plotted on the x-axis, showing the significance of the gene clusters.
(B) GO analysis of genes circadian in "both diets", "KD only" and "CC only" in IECs. The negative log (base 10) of the p value [-log10(pvalue)] was plotted on the x-axis, showing the significance of the gene clusters.
(C) Amplitude analysis of transcripts circadian in "both diets" in the liver. The percentage of the ratio between CC and KD amplitude obtained through JTK_CYCLE analysis has been used. In the graph the percentage of genes with amplitude higher, lower or equal to CC condition is reported. (Student's t-test: p<0.001 for KD>CC, p<0.001 for KD<CC).
(D) Amplitude analysis of transcripts circadian in "both diets" in IECs. In the graph the percentage of genes with amplitude higher, lower or equal to CC condition is reported. (Student's t-test: p<0.001 for KD>CC, p<0.001 for KD<CC).

Figure S3. Heat maps of circadian transcripts p<0.05. Related to Figure 1.

(A) Heat maps of rhythmic transcripts in "both diets", "KD only" and "CC only" in the liver (p<0.05).
(B) Heat maps of rhythmic transcripts in "both diets", "KD only" and "CC only" in IECs (p<0.05).

Gene expression of core clock genes and BMAL1 phosporylation. Related to section: "Limited Effect of KD on Core-Clock Gene Oscillation".

(C-D) qPCR of core clock genes *Bmal1, Cry1, Per2* and *Rev-erba* in liver (C) and ileum (D) of KD and CC fed mice (n=5 per time-point, per group; two-way ANOVA, Holm-Sidak post hoc, comparisons for factor: diet within ZT *p<0.05).
(E-F) Whole cell extract western blot in liver (E) and ileum (F) of KD and CC fed mice, showing no difference in BMAL1 protein expression and phosphorylation (Representative blot, n=3 per time-point, per group).
Error bars represent SEM.

Liver and IECs gene expression in *Clock* deficient mice upon KD. Related to Figure 3.

(G) *Nampt* and *Pnpla2* gene expression at ZT12 in the liver of *Clock* deficient mice fed to CC or KD (n=4-5 per time-point, per group; one-way ANOVA, All Pairwise Multiple Comparison (Student-Newman-Keuls) *p<0.05).
(H) *Nampt* and *Pnpla2* gene expression at ZT12 in IECs of *Clock* deficient mice fed to CC or KD (n=4-5 per time-point, per group; one-way ANO, All Pairwise Multiple Comparison (Student-Newman-Keuls), *p<0.05).

Figure S4. Analysis of BMAL1 target genes in liver and gut circadian transcriptome. Related to Figure 3.

(A) Heat-map of BMAL1 target genes, circadian in both CC and KD in liver (n=3 per time-point, per group, p<0.01, FDR<0.1).
(B) Heat-map of BMAL1 target genes, circadian in both CC and KD in IECs (n=3 per time-point, per group, p<0.01, FDR<0.1).
(C) Phase lag analysis of BMAL1 target genes, circadian in both CC and KD in hepatic tissue (Anderson-Darling test, phase distributions significance p<0.05).

(D) Phase lag analysis of BMAL1 target genes, circadian in both CC and KD in IECs (Anderson-Darling test, phase distributions significance $p<0.05$. Comparisons not shown: phase distribution difference in BMAL1 target genes upon KD: liver vs IECs $p<0.05$; phase distribution difference in BMAL1 target genes upon CC: liver vs IECs $p<0.05$).

(E) Percentage of the number of genes with increase, decrease or same level of expression in KD with respect to CC at ZT8 in liver. The gene expression mean value (n=3 animals per group) at ZT8 in CC or KD were used in this analysis. (Student's t-test: $p=0.05$ for KD>CC, $p=0.01$ for KD<CC).

(F) Percentage of the number of genes with increase, decrease or same level of expression in KD with respect to CC at ZT8 in IEC. (Student's t-test: $p=0.01$ for KD>CC, $p<0.001$ for KD<CC).

BMAL1 target gene expression and BMAL1 chromatin recruitment on target promoter regions. Related to Figure 3.

(G) *Nmnat3* gene expression and BMAL1 chromatin binding on its promoter region in the liver of CC and KD fed mice (n=5 per time-point, per group; two-way ANOVA, Holm-Sidak post hoc, comparisons for factor: diet within ZT *$p<0.05$).

(H) *Bhlhe41* gene expression and BMAL1 chromatin binding on its promoter region in the liver of CC and KD fed mice (n=5 per time-point, per group; two-way ANOVA, Holm-Sidak post hoc, comparisons for factor: diet within ZT *$p<0.05$).

(I) BMAL1 chromatin binding on the E-box in the promoter region of *Per2* and *Rev-erbα* genes (n=5 per time-point, per group; two-way ANOVA, Holm-Sidak post hoc, comparisons for factor: diet within ZT, no significant difference).
IgG represents ChIP experiment performed with an isotype matched control immunoglobulin (Normal rabbit IgG) to BMAL1.
Error bars represent SEM.

Acetyl K9-14 on histone H3 abundance on specific promoter regions at ZT0 and ZT12, in the liver. Realted to Figure 5.

(J) Liver ChIP of Acetylated (Acetyl) lysine (K) 9-14 on histone H3. qPCR showing the relative abundance of H3 Acetyl(K9-14) on the PPAR responsive element (PPRE) of specific promoter: *Hmgcs2, Acot2*, *Cpt1a* and *Angptl4* at ZT0 and ZT12 (n=3 per time point, per group; two-way ANOVA, Holm-Sidak post hoc, comparisons for factor, no significant difference).
Error bars represent SEM.

Figure S5. Major PPARα target genes circadian profile in IECs and liver. Related to Figure 4.

(A) Pie chart representing well-known PPARα targets belonging to specific biological pathway. The genes with a circadian profile in phase with PPARα nuclear accumulation in IECs are written close to every slice of the pie chart with the same color of the correspondent section. The circadian profile of these genes is represented in the heat maps in (B) and (C).

(B-C) Heat map of the targets in phase with PPARα nuclear accumulation in IECs (B) and heat map profile of the same genes in the liver (C) (Fisher's exact test $p < 0.01$).

Figure S6. βOHB levels influence histone acetylation specifically in the intestine. Related to Figure 5.

(A) Serum βOHB concentration levels at ZT8 and ZT20 in mice fed to CC or 1,3 butanediol diet (BD) for 4 weeks (n=5-6 per time point, per group; two-way ANOVA, Holm-Sidak post hoc, comparisons for factor: diet within ZT *$p<0.05$).

(B) Expression levels of PPARα target genes (*Hmgcs2*, *Acot2, Cpt1a* and *Angptl4*) in the liver of mice fed to CC or BD (n=5-6 per time point, per group; two-way ANOVA, Holm-Sidak post hoc, comparisons for factor: diet within ZT *$p<0.05$).

(C) H3 Acetyl(K9-14) abundance on the PPRE of *Hmgcs2, Acot2, Cpt1a* and *Angptl4* promoters in the liver upon CC or BD (n=5 per time point, per group; two-way ANOVA, Holm-Sidak post hoc, comparisons for factor: diet within ZT *$p<0.05$).

(D) Expression levels of *Hmgcs2*, *Acot2, Cpt1a* and *Angptl4* genes in the ileum of CC or BD fed mice (n=5-6 per time point, per group; two-way ANOVA, Holm-Sidak post hoc, comparisons for factor: diet within ZT *$p<0.05$).

(E) H3 Acetyl(K9-14) abundance on the PPRE of *Hmgcs2, Acot2, Cpt1a* and *Angptl4* promoters in the intestine upon CC or BD (n=5 per time point, per group; two-way ANOVA, Holm-Sidak post hoc, comparisons for factor: diet within ZT *$p<0.05$).
Error bars represent SEM.

Figure S7. Gene expression of core clock and clock output genes in liver and intestine of fructose and sucrose treated mice. Related to Figure 6.

(A) *Bmal1, cry1, Per2, Rev-erba, Dbp, Nampt* and *Pnpla2* gene expression in the liver of animals fed 4-week KD or CC and administered with fructose oral gavage (4g/Kg) once a day, per 7 days during the last week of dietary regimen (n=5 per time point, per group; two-way ANOVA, Holm-Sidak post hoc, comparisons for factor: diet within ZT *p<0.05).

(B) *Bmal1, cry1, Per2, Rev-erba, Dbp, Nampt* and *Pnpla2* gene expression in the intestine of animals fed 4-week KD or CC and administered with fructose oral gavage (4g/Kg) once a day, per 7 days during the last week of dietary regimen (n=5 per time point, per group; two-way ANOVA, Holm-Sidak post hoc, comparisons for factor: diet within ZT *p<0.05).

(C) *Bmal1, cry1, Per2, Rev-erba, Dbp, Nampt* and *Pnpla2* gene expression in the liver of animals fed 4-week KD or CC and treated with 30% sucrose in drinking water (n=5 per time point, per group; two-way ANOVA, Holm-Sidak post hoc, comparisons for factor: diet within ZT *p<0.05).

(D) *Bmal1, cry1, Per2, Rev-erba, Dbp, Nampt* and *Pnpla2* gene expression in the intestine of animals fed 4-week KD or CC and treated with 30% sucrose in drinking water (n=5 per time point, per group; two-way ANOVA, Holm-Sidak post hoc, comparisons for factor: diet within ZT *p<0.05).

Error bars represent SEM.